



1

2 **Designing global climate and atmospheric chemistry simulations for 1 km and 10**
3 **km diameter asteroid impacts using the properties of ejecta from the K-Pg impact**

4 Owen B. Toon¹, Charles Bardeen², Rolando Garcia²

5 ¹ Department of Atmospheric and Oceanic Science, Laboratory for Atmospheric and
6 Space Physics, University of Colorado, Boulder

7 ² National Center for Atmospheric Research, Boulder, Colorado

8 *Correspondence to:* O.B. Toon (toon@lasp.colorado.edu)

9

10 **Abstract.** About 66 million years ago an asteroid about 10 km in diameter struck the
11 Yucatan Peninsula creating the Chicxulub crater. The crater has been dated and found to
12 be coincident with the Cretaceous-Paleogene (K-Pg) mass extinction event, one of 6 great
13 mass extinctions in the last 600 million years. This event precipitated one of the largest
14 episodes of rapid climate change in Earth history, yet no modern three-dimensional
15 climate calculations have simulated the event. Similarly, while there is an on-going effort
16 to detect asteroids that might hit Earth and to develop methods to stop them, there have
17 been no modern calculations of the sizes of asteroids whose impacts on land would cause
18 devastating effects on Earth. Here we provide the information needed to initialize such
19 calculations for the K-Pg impactor and for a 1 km diameter impactor.

20 There is considerable controversy about the details of the events that followed the
21 Chicxulub impact. We proceed through the data record in the order of confidence that a
22 climatically important material was present in the atmosphere. The climatic importance
23 is roughly proportional to the optical depth of the material. Several hundred-micron
24 diameter spherules are found globally in an abundance that would have produced an
25 atmospheric layer with an optical depth around 20, yet their large sizes would only allow
26 them to stay airborne for a few days. They were likely important for triggering global
27 wildfires. Soot, probably from global or near-global wildfires, is found globally in an
28 abundance that would have produced an optical depth near 100, which would effectively
29 prevent sunlight from reaching the surface. Nanometer sized iron particles are also
30 present globally. Theory suggests these particles might be remnants of the vaporized
31 asteroid and target that initially remained as vapor rather than condensing on the
32 hundred-micron spherules when they entered the atmosphere. If present in the abundance
33 suggested by theory, their optical depth would have exceeded 1000. Clastics may be
34 present globally, but only the quartz fraction can be quantified since shock features can
35 identify it. However, it is very difficult to determine the total abundance of clastics. We
36 reconcile previous widely disparate estimates and suggest the clastics may have had an
37 optical depth near 100. Sulfur is predicted to originate about equally from the impactor
38 and from the Yucatan surface materials. By mass, sulfur is less than 10 percent of the
39 mass of the spheres and nano-particles. Since the sulfur probably reacted on the surfaces
40 of the soot, nano-particles, clastics and spheres, it is likely a minor component of the
41 climate forcing; however, detailed studies of the conversion of sulfur gases to particles
42 are needed to determine if sulfuric acid aerosols dominated in late stages of the evolution



43 of the atmospheric debris. Numerous gases, including CO₂, SO₂ (or SO₃), H₂O, CO₂, Cl,
44 Br, and I, were likely injected into the upper atmosphere by the impact or the immediate
45 effects of the impact such as fires across the planet. Their abundance might have
46 increased relative to current ambient values by a significant fraction of current values for
47 CO₂, and by factors of 100 to 1000 for the other gases.

48 For the 1 km impactor, nano-particles might have had an optical depth of 1.5 if the
49 impact occurred on land. If the impactor struck a densely forested region, soot from the
50 forest fires might have had an optical depth of 0.1. Only S and I would be expected to be
51 perturbed significantly relative to ambient gas phase values. 1 km asteroids impacting
52 the ocean may inject seawater into the stratosphere as well as halogens that are dissolved
53 in the seawater.

54 For each of the materials mentioned we provide initial abundances and injection altitudes.
55 For particles we suggest initial size distributions and optical constants. We also suggest
56 new observations that could be made to narrow the uncertainties about the particles and
57 gases generated by large impacts.

58

59 **Keywords** Climate modeling; Initial conditions; Asteroid impacts; K-Pg extinction

60

61 **1. Introduction and definitions**

62 About 66 million years ago an asteroid around 10 km in diameter hit the Earth near the
63 present day Yucatan village of Chicxulub and created an immense crater whose age
64 coincides with the Cretaceous-Paleogene (K-Pg) global mass extinction (Alvarez et al.,
65 1980; Schulte et al., 2010; Renne et al., 2013). There is an enormous literature
66 concerning this event and its aftermath. Surprisingly, however, there are very few papers
67 about the changes in climate and atmospheric chemistry caused by the debris from the
68 impact while it was in the atmosphere, and no studies based on modern three-dimensional
69 climate models. Nevertheless, this event was almost certainly one of the largest and most
70 dramatic short-term perturbations to climate and atmospheric chemistry in Earth history.

71 There is substantial evidence for many other impacts in Earth history as large or larger
72 than that at Chicxulub, mostly in the Pre-Cambrian (e.g. Johnson and Melosh, 2012a;
73 Glass and Simonson, 2012). There is also a growing effort to find asteroids smaller than
74 the one that hit Chicxulub, but whose impact might have significant global effects, and to
75 develop techniques to stop any that could hit the Earth. For example, as of November 17,
76 2015 NASA's Near Earth Object Program identifies 13,392 objects whose orbits pass
77 near Earth. Among these objects, 878 have a diameter of about 1 km or larger, and 1640
78 have been identified as Potentially Hazardous Asteroids, which are asteroids that pass the
79 Earth within about 5% of Earth's distance from the sun, and are larger than about 150 m
80 diameter.

81 There is evidence for such smaller impacts in recent geologic history from craters,
82 osmium variations in sea cores (Paquay et al., 2008), and spherule layers (Johnson and
83 Melosh, 2012a; Glass and Simonson, 2012). For instance, a multi-kilometer object
84 formed the Siberian Popigai crater in the Late Eocene and another multi-kilometer object



85 formed the Late Eocene Chesapeake Bay crater in the United States. Size estimates vary
86 between techniques, but within a given technique the Popigai object is generally given a
87 diameter half that of the Chicxulub object. Toon et al. (1997) point out that the effects of
88 impacts scale with the impactor energy, or cube of the diameter, not diameter (or crater
89 size). The Popigai object likely had about 12% of the energy of the Chicxulub object.
90 Surprisingly, except for collisions in the ocean (Pierazzo et al., 2012), climate models
91 have not been used to determine the destruction that might be caused by objects near 1
92 km in diameter, a suggested lower limit to the size of an impactor that might do
93 significant worldwide damage (e.g. Toon et al., 1997).

94 Here we describe the parameters that are needed to initialize three-dimensional climate
95 and atmospheric chemistry models for the Chicxulub impact and for a 1-km diameter
96 asteroid impact. Nearly every aspect of the K-Pg impact event is uncertain, and
97 controversial. We will address some of these uncertainties and controversies and make
98 recommendations for the initial conditions that seem most appropriate for a climate
99 model, based upon the geological evidence. We will also suggest the properties of the
100 initial impact debris from a 1 km diameter asteroid.

101 There are numerous observed and predicted components of the Chicxulub impact debris.
102 The distal debris layer, defined to be the debris that is more than 4000 km removed from
103 the impact site, is thought to contain material that remained in the atmosphere long
104 enough to be globally distributed. This distal layer, sometimes called the fireball layer or
105 the magic layer, is typically only a few mm thick (Smit, 1999). As discussed below, the
106 layer includes 200 μm -sized spherules, 50 μm -sized shocked quartz grains, 0.1- μm -sized
107 soot and a 20 nm-sized iron-rich material.

108 We discuss each of the components of the distal layer in detail below. As an outline of
109 this discussion we find the following: The large spherules are not likely to be of
110 importance to the climate because they would have been removed from the atmosphere in
111 only a few days. However, they may have initiated global wildfires. The shocked quartz
112 grains, one of the definitive pieces of evidence for an impact origin as opposed to
113 volcanic origin of the debris layer, is likely only a small fraction of the clastic debris. It
114 is difficult to identify the rest of the minerals produced by crushing because there is
115 material in the layer that might have been produced long after the impact by erosion and
116 chemical alteration of the large spheres or from the ambient environment. One major
117 controversy surrounding the clastic material is the fraction that is submicron-sized.
118 Particles larger than a micron will not remain in the atmosphere very long and, therefore,
119 are less likely to affect climate. Unfortunately, the sub- μm micron portion of the clastics
120 in the distal layer, which might linger in the atmosphere for a year or more, has not been
121 directly measured. Our estimate of the mass of submicron-sized clastics suggest that it
122 could have had a very high large optical depth that would be capable of modifying the
123 climate significantly. Nevertheless, submicron clastics are only of modest climatic
124 importance relative to the light absorbing soot and possibly the iron rich nm-scale debris.
125 Submicron soot is observed in the global distal layer in such quantity that it would have
126 had a very great impact on the climate when it was suspended in the atmosphere. The
127 major controversy surrounding the soot is whether it originated from forest fires, or from
128 hydrocarbons at the impact site. The origin of the soot, however, is of secondary
129 importance with regard to its effect on climate. Since the soot layer overlaps the iridium



130 layer in the distal debris it had to have been created within a year or two of the impact,
131 based on the removal time of small particles from the atmosphere (and ocean), and could
132 not have been the result of fires long after the impact. The fireball layer is often colored
133 red and contains abundant iron. Some of the iron has been identified as part of a 20 nm-
134 sized particle phase, possibly representing a portion of the recondensed vaporized
135 impactor and target. However, relatively little work has been done on this material. Its
136 abundance has not been measured, but theoretical work suggests its mass could have been
137 comparable to that of the impactor. Therefore, the nm-sized particles could have been of
138 great importance to the climate. Each of the materials just described is present in the
139 distal layer, and their impacts on the atmosphere were likely additive.

140 There are several other possible components of the distal layer that have not been clearly
141 identified and studied as part of the impact debris, which we discuss below. Water,
142 carbon, sulfur, chlorine, bromine, and iodine were likely present in significant quantities
143 in the atmosphere after the impact. The Chicxulub impact occurred in the sea with depths
144 possibly ranging up to 1 km. The target sediments and the asteroid probably also
145 contained significant amounts of water. Water is an important greenhouse gas, and could
146 condense to form rain, which might have removed materials from the stratosphere.
147 Carbon is present in seawater, in many asteroids and in sediments. Injections as carbon
148 dioxide or methane might have led to an increased greenhouse effect. Sulfur is widely
149 distributed in the ambient environment, and is water-soluble. Therefore, it is difficult to
150 identify extraterrestrial sulfur in the debris layer. However, the impact site contains a lot
151 of sulfur, and asteroids also contain significant amounts of sulfur. Sulfur is noteworthy
152 because it is known to produce atmospheric particulates in today's atmosphere that alter
153 the climate. Chlorine, bromine and iodine can destroy ozone, and their effectiveness as
154 catalysts is enhanced by heterogeneous reactions on sulfuric acid aerosols.

155 In addition to the mm-thick distal layer, there is an intermediate region ranging from
156 2,500-4,000 km from the impact site with a debris layer that is several cm thick (Smit,
157 1999). This layer contains microtektites (molten rock deformed by passage through the
158 air), shocked quartz, as well as clastics such as pulverized and shocked carbonates. Most
159 of this layer originated from the target material in the Yucatan. It is of interest because,
160 like the debris clouds from explosive volcanic eruptions, components of this material
161 may have escaped from the region near the impact site to become part of the global debris
162 layer.

163 Properties of each of these materials need to be known in order to model their effects on
164 the climate and atmospheric chemistry realistically. These properties include the altitude
165 of injection, the size of the injected particles, the mass of injected particles or gases, the
166 density of the particles, and the optical properties of the injected particles and gases. Our
167 best estimates for these properties for the K-Pg impact are summarized in Table 1 for
168 particles and Table 2 for gases, and discussed for each material in Section 2. Tables 3
169 and 4 provide an extrapolation of these properties for an impact of by a 1 km sized object.

170 While the mass of the injected material is useful as an input parameter to a model, the
171 optical depth of the particles is needed to quantify their impact on the atmospheric
172 radiation field and, therefore, on the climate. Hence, optical depth is a useful quantity to
173 compare the relative importance of the various materials to the climate. For a



174 monodisperse particle size distribution, the optical depth is given by $\tau = \frac{3Mq_{\text{ext}}}{4\rho r}$. Here M
175 is the mass of particles in a column of air (for example, g cm^{-2}), r is the radius of the
176 particles, ρ is the density of the material composing the particles, and q_{ext} is the optical
177 extinction efficiency at the wavelength of interest. The optical extinction efficiency is a
178 function of the size of the particles relative to the wavelength of light of interest, and of
179 the optical constants of the material. The optical extinction efficiency is computed
180 accurately in climate models. However, a rough value of q_{ext} for particles larger than 1
181 μm , is about 2 for visible wavelength light. We use this rough estimate for q_{ext} in Table
182 1 and Table 3 to calculate an optical depth for purposes of qualitatively comparing the
183 importance of the various types of injected particles. We assume in the heuristic
184 calculations of optical depth in Tables 1 and 3 that the particles have a radius of 1 μm
185 because smaller particles will quickly coagulate to a radius near 1 μm given the large
186 masses of injected material.

187 Below we define the properties that are needed to perform climate or atmospheric
188 chemistry simulations for each material that might be important.

189

190 2. Particulate Injections

191 2.1 Large spherules

192 2.1.1 Large spherules from the Chicxulub impact

193 The most evident component of the distal and regional debris layers is spherical particles,
194 some of which are large enough to be seen with the naked eye. Due to their spherical
195 shape it is assumed that they are part of the melt debris from the impact or the condensed
196 vapor from the impact (Johnson and Melosh, 2012b; 2014). The particles are not thought
197 to have melted on reentry into the atmosphere since debris launched above the
198 atmosphere by the impact should not reach high enough velocities to melt when it
199 reenters the atmosphere. According to Bohor and Glass (1995) there are two types of
200 spherules, with differing composition and distribution. They identify Type 1 splash-form
201 spherules (tektites or microtektites) that occur in the melt-ejecta (basal or lower) layer of
202 the regional debris layer where it has a two-layered structure. These spherules are found
203 as far from the Chicxulub site as Wyoming, but generally do not extend beyond about
204 4000 km away from Chicxulub. While the type 1 particles are derived from silicic rocks,
205 they are also mixed with sulfur rich carbonates from the upper sediments in the Yucatan.
206 The Type 1 spherules are poor in Ni and Ir, and the lower layer is poor in shocked quartz,
207 consistent with their origin from the low energy impact ejecta from the crater. Generally
208 the debris layer within about 4000 km of the crater is almost entirely composed of target
209 material, rather than material from the impactor itself. Type 2 spherules, on the other
210 hand, are found in the distal debris layer, and presumably formed primarily from the
211 condensation of rock vapor from the impactor and target (O'Keefe and Ahrens, 1982;
212 Johnson and Melosh, 2012b). There are sub-types of Type 2 spherules that correspond to
213 varying composition of the original source material. Type 2 spherules occur in the upper
214 layer in impact sites near Chicxulub, which merges into the fireball layer at distal sites.



215 The Type 2 spherules are rich in Ni and Ir, while the fireball layer is rich in shocked
216 quartz.

217

218 The formation of the spherical particles may depend on two different processes. Melosh
219 and Vickery (1991) describe one formation mechanism, probably occurring in less
220 heavily shocked portions of the target, when molten material decompresses until it
221 reaches a critical line at which it starts to boil. The gas drag from the rock vapor on the
222 molten rock spheres then tears apart the molten material, just as water droplets break
223 apart when they fall through air. The relative velocities of water drops in air and the melt
224 in vapor are similar, as are the surface tensions. As a result melt droplets are similar in
225 size to drizzle drops in light rain, near $250\ \mu\text{m}$. According to Johnson and Melosh
226 (2012b) these spherical particles are most likely to be found within 4000 km of the
227 impact site, and to be chemically related to the target material, and not to the impactor.
228 Such materials are reported across North America as Type 1 spherules (Bohor et al.,
229 1987), and are sometimes referred to as microtektites. Since these spherules are not
230 global, they likely were not as relevant to climate as the Type 2 spherules.

231

232 Melt droplets can also form in heavily shocked parts of the impact debris as rock vapor
233 condenses to form melt in the fireball, which rises thousands of km above the Earth's
234 surface. These melt droplets form the Type 2 spherules. O'Keefe and Ahrens (1982) first
235 modeled this process, and deduced that particles near a few hundred microns in size
236 would form, as is observed. They also pointed out that the size of the spheres would be
237 proportional to the size of the impactor. Johnson and Melosh (2012b) recently
238 reconsidered this process for forming melt particles. They point out that the large
239 spherules contain iridium (e.g., Smit, 1999), which is consistent with them being
240 composed partially of the vaporized impactor. Their model of the formation and
241 distribution of these particles suggests the particles have a size that varies spatially over
242 the plume. Averaging over the plume yields a mean size of $217\ \mu\text{m}$ with a standard
243 deviation of about $47\ \mu\text{m}$ for a 10 km diameter impactor hitting at $21\ \text{km s}^{-1}$. From the
244 two examples given by Johnson and Melosh (2012b) it appears that the standard
245 deviation is consistently 22% of the mean radius for asteroids of different sizes. The
246 initial values for the various properties of Type 2 spherules described above are
247 summarized in Table 1 for the K-Pg impactor.

248

249 Smit (1999), who refers to the Type 2 spherules in the distal layer as microkrystites,
250 estimated that these particles typically have a diameter near $250\ \mu\text{m}$, and a surface
251 concentration of about 20,000 particles cm^{-2} over the Earth. Unfortunately, we are not
252 aware of studies that measure the dispersion of the size distribution, or the spatial
253 variation of the abundance of these particles. We assume that the particles have the
254 density of CM2 asteroids, since Cr isotope ratios suggest that is the composition of the K-
255 Pg impactor (Trinquier et al., 2006). Assuming this density, $\sim 2.7\ \text{g cm}^{-3}$, the mass of
256 spherules per unit area of the Earth is about $0.4\ \text{g cm}^{-2}$, and the initial optical depth is
257 about 20, as noted in Table 1. These spherules compose about half of the mass of the
258 distal layer. We assume the particles were initially distributed uniformly around the
259 globe, with the initial mixing ratio in the atmosphere varying only in altitude. Some
260 theoretical studies, such as Kring and Durda (2002) and Morgan et al. (2013), suggest



261 that these particles were not uniformly deposited in latitude and longitude, but had
262 focusing points such as the antipodes of the impact site. Unfortunately, we are not aware
263 of quantitative data on the global distribution of the spherules. The study by Morgan et
264 al. (2013) may also be more applicable to the Type 1 spherules since their numerical
265 model does not produce vaporized impactor.

266 According to the simulations of Goldin and Melosh (2009), the in-falling spherical
267 particles reached terminal fall velocity at ~70km altitude, at which point they begin to
268 behave like individual airborne particles. Kalasnikova et al. (2000) investigated
269 incoming micrometeorites in the present atmosphere, which generally ablate near 85 km.
270 Kalasnikova et al. (2000) find material entering from space stops in the atmosphere after
271 it encounters a mass of air approximately equal to its own mass. Therefore, the altitude
272 distribution is taken to be Gaussian, centered at 70 km and with a half-width of one
273 atmospheric scale height (about 6.6 km based on the U.S. Standard Atmosphere). A scale
274 height is chosen as the half width of the injection profile since it is a natural measure of
275 the density of the atmosphere. Figure 1 illustrates the vertical injection profile of the
276 spherules (green curve). As discussed below we expect several materials with origins
277 similar to those of the spherules to be injected in this same altitude range, but others with
278 origins unrelated to the impact generated plume, such as soot from fires, to be injected at
279 lower altitudes.

280

281 The energy release from the reentry of these large spherical particles into the atmosphere
282 was likely responsible for setting most of the above ground terrestrial biosphere on fire.
283 However, due to their size, the spherules could not have remained in the atmosphere for
284 more than a few days. Hence they likely did not have a significant direct impact on the
285 climate, but fell to Earth like a gentle rain.

286

287 **2.1.2 Large spherules from a 1 km diameter asteroid impact**

288 Like O'Keefe and Ahrens (1982), Johnson and Melosh (2012b) conclude that the particle
289 size will vary in proportion to the impactor diameter. For a 1 km diameter impactor
290 hitting the land they suggest that the mean diameter of the spherical particles will be
291 about 15 μm . Table 3 provides our assumed properties of the spherules from a
292 hypothetical 1 km diameter impactor hitting the land. It is likely that spherules would be
293 distributed over much of the globe even for the 1 km diameter impact. Johnson and
294 Melosh (2012a) as well as Glass and Simonson (2012) report a spherule layer associated
295 with the Popagai impact in the late Eocene. This layer contains spherules similar in size
296 or even larger than those associated with the Chicxulub impact. However, this layer is
297 only about 10% as thick as the distal layer from the Chicxulub impact. A 1 km impactor
298 hitting the deep oceans may not produce a layer of spherules.

299

300 **2.2 Soot**

301 **2.2.1 Soot from the Chicxulub impact**

302 Spherical soot (also referred to as black carbon, or elemental carbon) particles were
303 discovered in the boundary layer debris at sites including Denmark, Italy, Spain, Austria,
304 Tunisia, Turkmenistan, the United States and New Zealand by Wolbach et al. (1985;



305 1988; 1990). Soot was also found in anaerobic deep-sea cores from the mid-Pacific
306 (Wolbach et al., 2003). Soot was apparently lost by oxidation in aerobic deep-water sites
307 in the 66 million years since emplacement. There is debate about whether these particles
308 originated from global wildfires, or from the impact itself (Belcher et al., 2003, 2004,
309 2005, 2009; Belcher, 2009; Harvey et al., 2008; Robertson et al., 2013a, Pierazzo and
310 Artemieva (2012), Premovic (2012), Morgan et al. (2013)). Robertson et al. (2013) and
311 the other more recent papers, argue that it is implausible that there was enough carbon at
312 the impact site to produce the amount of soot observed by Wolbach et al. (1988). This
313 debate about the origin of the particles does not greatly affect the effect these particles
314 would have had on the climate when they were suspended in the atmosphere. The
315 particles are small and widely distributed, and so must have remained in the atmosphere
316 for a few years. They are numerous and so must have produced a very large optical depth
317 and, being composed of carbon, they would have been excellent absorbers of sunlight.
318 Whether the soot particles originated from global fires and were deposited in the upper
319 troposphere, or they originated at the impact site and were deposited in the mesosphere,
320 the climate effect of the observed soot would have been very great. Some have suggested
321 that the soot resulted from wildfires in dead and dying trees that occurred well after the
322 impact. However, Wolbach et al. (1988) show that soot and iridium are tightly correlated
323 and collocated. The soot and iridium in the distal layer must have been deposited within
324 a few years of the impact, since small particles will not stay in the air much longer.
325 Therefore, any fires must have been very close in time to the impact.

326
327 Wolbach et al. (1988) estimated the global mass of soot in the debris layer as $7 \pm 4 \times 10^{16}$ g
328 of C or equivalently 1.3×10^{-2} g C cm⁻². This mass of soot would require that the bulk of the
329 above ground biomass burned and was partially converted to soot with an efficiency of 3%,
330 assuming the biomass is 1.5 g C cm⁻² of above ground, dry organic mass per cm² over the
331 land area of Earth, which is typical of current tropical forests. This inferred 3% emission
332 factor is about 60 times greater than that suggested by Andreae and Merlet (2001) for
333 current wildfires, but agrees with laboratory and other observations from burning wood
334 under conditions consistent with mass fires (Crutzen et al., 1984; Turco et al., 1990). The
335 high soot emission efficiency inferred for the K-Pg impact likely represents the processes
336 occurring in firestorms, also called mass fires, set globally after the impact as opposed to
337 the processes observed in typical forest fires and discussed by Andreae and Merlet (2001).
338 Mass fires are more intense than forest fires, and consume all the fuel available, possibly
339 including that in the near surface soil. Ivany and Salawitch (1993) argued independently
340 from oceanic carbon isotope ratios that at least 25% of the above ground biomass must
341 have burned at the K-Pg boundary.

342
343 As noted in Table 1, the mass of soot found by Wolbach et al. (1988) would produce an
344 optical depth near 100 if the particles coagulated to spheres with a radius of 1 μm while
345 they were in the atmosphere. Toon et al. (1997) pointed out that soot clouds with such a
346 large optical depth would reduce light levels at the Earth's surface effectively to zero. The
347 optical and chemical evolution of the particles once in the atmosphere may be influenced
348 by the presence of liquid organics on the soot particles. Bare soot particles coagulate into
349 chains and sheets, while particles that are coated by liquids may form balls. Chains,
350 sheets, and coated balls have very different optical properties than do spheres (Wolf and



351 Toon, 2010; Ackerman and Toon, 1981; Bond and Bergstrom, 2006; Mikhailov et al.,
352 2006). Particulate organic matter can be absorbing, and soot coated with organics can
353 have enhanced absorption relative to soot that is uncoated (Lack et al., 2012; Mikhailov
354 et al., 2006). These fractal shapes, and organic coatings might not be preserved in samples
355 in the distal layer since all the particles have been consolidated in a layer, and even in the
356 current atmosphere the organics have short lifetimes due to rapid oxidation.

357
358 Wolbach et al. (1985) fit the size of the particles they observed, after exposing them to
359 ultrasound to break up agglomerates, to a lognormal size distribution, described by

$$361 \quad \frac{dN}{d \ln r} = \frac{N_t}{\ln \sigma \sqrt{2\pi}} \exp\left[-\ln^2\left(\frac{r}{r_m}\right) / 2 \ln^2 \sigma\right]. \quad (1)$$

362
363 Here r is the particle radius, N_t is the total number of particles per unit volume of air, r_m is
364 the mode radius, and σ is the width of the distribution. Wolbach et al. (1985) find $r_m =$
365 $0.11 \mu\text{m}$, and $\sigma = 1.6$ for the soot in the K-Pg boundary layer. We assume this
366 distribution represents the initial sizes of the soot particles. The final size, which would
367 be determined by coagulation while in the atmosphere, might not be preserved in the
368 sediments, and loosely bound clumps of particles would have been destroyed by the
369 ultrasound treatment of the samples.

370
371 The size distribution of soot from the K-Pg boundary is similar to that of smoke nearby
372 present day biomass fires as indicated in Fig. 2 (e.g., Matichuk et al., 2008). This
373 similarity in sizes is somewhat surprising because the present day smoke size distribution
374 includes organic carbon, which is present in addition to the elemental carbon (soot).
375 Generally, in wildfire smoke organic carbon has 5-10 times the mass of soot, so one
376 might anticipate that the K-Pg soot would be about half the size of the present day smoke
377 rather than of similar size since the organic coatings are no longer present, or were never
378 present, on the K-Pg soot. The organics might never have been present, because mass
379 fires are very intense and tend to consume all the available fuel, which might include the
380 organic coatings. Aggregation in the hot fires may have caused this slightly larger than
381 expected size in the K-Pg sediments. Wolbach et al. (1985) suspended their samples in
382 water and subjected them to ultrasound for 15 minutes in a failed attempt to completely
383 break up agglomerates. This failure indicated that the remaining agglomerates might
384 have been flame-welded. Therefore, the K-Pg size distribution from Wolbach et al.
385 (1985) does not represent the monomers in the aggregate soot fractal structures. Rather
386 the K-Pg size distributions represent a combination of monomers and aggregates that may
387 have formed at high temperatures. Possibly the smallest sized particles measured by
388 Wolbach et al. (1985), which have radii of 30-60 nm, represent the soot monomers.
389 These are in the same general range as monomer sizes observed in soot from
390 conventional fires (Bond and Bergstrom, 2006).

391
392 The injection altitude of the soot depends on its source. In a series of papers Belcher et
393 al. (2003; 2004; 2005; 2009) and Belcher (2009) argued from multiple points of view that
394 there were no global forest fires, and Harvey et al. (2008) argued that the soot originated
395 from oil, coal and other organic deposits at the location of the impact. If correct, the soot



396 might have been injected at high altitude along with the large spherules. Recently,
397 Robertson et al. (2013a) reconsidered each of the arguments presented by Belcher et al.
398 and came to the conclusion that global wildfires did indeed occur. Pierazzo and
399 Artemieva (2012), Premovic (2012), Morgan et al. (2013), as well as Robertson et al.
400 (2013a) have independently argued that oil and other biomass in the crater is
401 quantitatively insufficient to be the source of the soot. Therefore, we assume that the
402 soot indeed originated from burning biomass distributed over the globe. The soot is
403 clearly present in the distal layer material, and therefore was once in the atmosphere
404 where it could cause significant changes to the climate.

405

406 Toon et al. (2007) have outlined the altitudes where one expects large mass fires to inject
407 their smoke. Numerical simulations have shown that mass fires larger than about 5 km in
408 diameter have smoke cloud tops well into the stratosphere. The smoke itself is
409 distributed over a range of heights, however. The details of the injection profiles depend
410 on the rate of fuel burning, the size of the fires, and the meteorological conditions among
411 other factors. In addition, some smoke is quickly removed from the atmosphere by
412 precipitation in pyro-cumulus. However, it is thought that over-seeding of the clouds by
413 smoke prevents precipitation, and that only 20% or so of the smoke injected into the
414 upper atmosphere is promptly rained out (Toon et al., 2007). Smoke that is injected near
415 the ground, on the other hand, will be removed by rainfall within days of weeks.

416

417 The K-Pg impact occurred at a time when average biomass density likely was higher than
418 now. Following Small and Heikes (1988; Figure 3f) and Pittcock et al. (1989) one would
419 expect smoke from large area fires burning in high biomass density areas to show a bi-
420 modal smoke injection profile. The smoke at higher levels is injected in the pyro-
421 cumulus and other regions with strong vertical motions. However, once the fires die-
422 down smoke will be emitted in the boundary layer. There are also downdrafts, as well as
423 entrainment and mixing with the environment, that occur in all cumulus and these will
424 carry some smoke into the boundary layer. We simulate this with injections whose
425 vertical distributions are Gaussian functions centered at the tropopause and at the surface,
426 as illustrated in Fig. 1. The injection at the tropopause has a half width of 3 km, but
427 nothing is injected above about 25 km. We set this upper altitude limit based on the
428 heights of the stratospheric sulfate clouds from explosive volcanic eruptions, which rise
429 buoyantly as do smoke plumes. The Gaussian distribution at the ground has a half width
430 of 1 km, assuming that the local boundary layer is relatively shallow. We assume 50%
431 of the soot is contained in each of these distributions for the general case. For the K-Pg,
432 we assume the soot observed in the distal layer was all in the portion of the Gaussian
433 distribution at the tropopause.

434 Therefore, the injection profile is given by:

435

436
$$I(g s^{-1} km^{-1}) = \frac{I_T}{2\sqrt{2\pi}} \left[\frac{1}{\mu} e^{-0.5\left(\frac{z}{\mu}\right)^2} + \frac{1}{\eta} e^{-0.5\left(\frac{z-z_{trop}}{\eta}\right)^2} \right] \quad (2)$$

437



438 Here I is the mass emission rate per km of altitude, I_T is the total mass emitted per second
439 after correcting for the emission altitude range (0-25 km) and grid spacing, μ is 1 km, η is
440 3 km, and z_{trop} is the altitude of the tropopause.

441

442 Geographically, we assume for the K-Pg event that all the surface biomass is set on fire.
443 For the 1 km diameter impact, however, only the region near the impact site would burn
444 as discussed further below.

445

446 There is also an issue of how long it takes to inject the smoke. Forest fires often burn for
447 days, advancing along a fire front as winds blow embers far beyond the flames and onto
448 unburned terrain. Mass fires may not spread because powerful converging winds restrict
449 the spread. However, little is known observationally about mass fires, and fires can
450 spread by intense infrared radiation lighting adjacent material. If mass fires are restricted
451 then they will burn only as long as they have fuel. The present above ground global
452 biomass in tropical forests is in the range of 0.6-1.2 g C cm⁻² (Houghton, 2005). The
453 energy content of biomass is on the order of 3x10⁴ J/g C or, given the biomass
454 concentration just mentioned, about 3x10⁸ J m⁻². Penner et al. (1986) and Small and
455 Heikes (1988) found that large area mass fires with energy release rates of 0.1 MW m⁻²
456 would have plumes reaching the lower stratosphere. Hence, it would be necessary to
457 assume that the fuel burned in an hour or so to achieve these energy releases. Of course,
458 it might take some time for fires in different places to start fully burning, so considering
459 the entire region of the mass fire, as opposed to a small individual part of the fires, might
460 prolong the energy release considerably. For example, it took several hours for the mass
461 fire in Hiroshima to develop after the explosion of the atom bomb (Toon et al., 2007)

462

463 It should be noted that in simulations of stratospheric injections of soot from nuclear
464 conflicts, soot is self-lofted by sunlight heating the smoke (Robock et al., 2007b).
465 However, in the case of the K-Pg impact, if there are other types of particles injected
466 above the soot, which then block sunlight, the soot may not be self-lofted, which will
467 limit its lifetime. The initial soot distribution that is estimated here does not include the
468 effects of self-lofting, which would continue after the initial injection and should be part
469 of the climate simulation.

470

471 The final property to specify for soot is the optical constants. This issue is complicated
472 by the possible presence of organic material on the soot (Lack et al., 2012). However, it
473 is known that many of these organics are quickly oxidized by ozone, which is plentiful in
474 the ambient stratosphere. The stratosphere after the impact however, may have become
475 depleted in ozone very quickly, so that the organic coatings might have survived. It is
476 also possible that intense fires, such as mass fires, will consume the organic coatings,
477 which may explain why the production of soot in the fires seems to have been so much
478 more efficient than for normal fires. It may therefore be sufficient to treat the soot as
479 fractal agglomerates of elemental carbon (Bond and Bergstrom, 2006). It is known that
480 the optical properties of the agglomerates will not obey Mie theory. However, one may
481 treat their optical properties as well as their microphysical properties using the fractal
482 optics approach described by Wolf and Toon (2010). The optical constants for elemental
483 carbon may then be used for the monomers. Alternatively, one may add the organic mass



484 to the particles, and treat them using core-shell theory (Toon and Ackerman, 1981;
485 Mikhailov et al., 2006).

486

487 Bond and Bergstrom (2006) have thoroughly reviewed the literature on the optical
488 properties of elemental carbon. They conclude that the optical constants are most likely
489 independent of wavelength across the visible, with a value that depends on the bulk
490 density of the particles. Following their range of values for refractive index versus
491 particle density we suggest using a wavelength independent real index of refraction
492 $n=1.80$ and an imaginary index $k=0.67$. We also use these values in the infrared as
493 shown in Figure 3. For the monomers in Tables 1 and 3, we adopt the density suggested
494 by Bond and Bergstrom (2006) for light absorbing material, 1.8 g cm^{-3} .

495

496 **2.2.2 Soot from a 1 km impact**

497 Extrapolations of the soot injection parameters to smaller impactors than the one defining
498 the K-Pg boundary should only involve changes to the mass of soot injected, since the
499 basic properties of the soot at the K-Pg boundary are similar to those of forest fire soot.
500 Therefore, the particle sizes, injection heights, and optical constants recommended in
501 Table 3 for the smaller impact are the same as listed in Table 1 for the Chicxulub impact.
502 The mass of soot injected is estimated from the extrapolations in Toon et al. (1997). For
503 an impactor as small as 1 km diameter, debris from the impact site would not provide
504 sufficient energy to ignite the global biota since the energy of the 1 km impactor is about
505 1000 times less than that of the Chicxulub impactor. Instead, radiation from the ablation
506 of the incoming object and from the rising fireball at the impact site would ignite material
507 that is within visible range of the entering object and the fireball. This ignition
508 mechanism is well understood from nuclear weapons tests (Turco et al., 1990). Hence,
509 for a 1 km diameter impactor the fuel load at the site of the impact becomes critical to
510 evaluate the soot release. No soot would be produced from an impact in the ocean, an ice
511 sheet, or a desert. In Table 3 to compute the smoke emitted (28 Tg), we use equation 12
512 from Toon et al. (1997) to obtain an area of $4.1 \times 10^4 \text{ km}^2$ for the expected area exposed to
513 high thermal radiation density from the fireball for a 1 km diameter impactor with an
514 assumed energy of $6.8 \times 10^4 \text{ Mt}$. We then multiply that area by 3% (the fraction of C in the
515 burned fuel that is converted to smoke) and by 2.25 g C cm^{-2} , (the assumed carbon
516 content per unit area of the dry biomass that burns). The user of Table 3 can choose
517 alternate values of the injected soot by scaling linearly to the biomass concentration they
518 chose.

519

520 Ivany and Salawitch (1993) suggest that the land average above ground biomass was about
521 $1 \times 10^{18} \text{ g}$ (about 0.7 g C cm^{-2}) at the end of the Cretaceous. The current land average above
522 ground biomass is about 0.3 to 0.44 g C cm^{-2} (Ciais et al., 2013). An additional 1 to 1.6 g C
523 cm^{-2} is currently present in the soil, while Ivany and Salawitch suggest 1 g C cm^{-2} in the soil
524 in the Cretaceous. Some of the soil biomass may burn in a mass fire. Tropical and boreal
525 forests currently have average biomass concentrations (above ground and in soil) of about
526 2.4 g C cm^{-2} , while temperate forests have about 1.6 g C cm^{-2} including soil carbon (Pan et
527 al., 2011). Soil carbon is 30% of carbon in tropical forests and 60% in boreal forests.
528 Together tropical and boreal forests cover 6% of the Earth's surface, and temperate forests



529 1.5%. These forests cover 26% of Earth's land area. In Table 3 we assume that the
530 biomass that burns is typical of a tropical or boreal forest assuming the soil carbon burns.
531 The reader can make other choices for the biomass by scaling from the fuel load that the
532 reader prefers.

533

534 Another modeling issue of concern is the ability of models to follow the initial evolution
535 of the plume. If we assume that half of the 28 Mt of smoke from the 1 km impact is
536 injected over an area of $4 \times 10^4 \text{ km}^2$, and over a depth of 6 km near the tropopause as 0.1
537 μm radius smoke particles, the smoke will have an initial optical depth near 4000, and the
538 number density of particles will be about 10^7 cm^{-3} . (The other half of the smoke mass
539 injected near the ground will likely be removed quickly and have little impact on
540 climate). Intense solar heating at the top of the smoke cloud near the tropopause will push
541 it upward, while coagulation will reduce the number of particles by a factor of 2 and
542 increase their size proportionately in only one minute. Hence, one needs to model this
543 evolution on sub-minute time scales to accurately follow the initial evolution.
544 Alternatively, but less accurately, one might spread out the injection in time and space, so
545 that the climate model can track the evolving smoke cloud using typical model time
546 steps.

547

548 **2. 3 Nano-particles from vaporized impactors**

549 **2.3.1 Nano-particles from the vaporized material following the Chicxulub impact**

550 Johnston and Melosh (2012b) calculate that about 44% of the rock vapor that was created
551 from the K-Pg asteroid impact remained as vapor rather than condensing to form large
552 spherules in the rising fireball. This vapor is about an equal mixture of impactor and
553 asteroid, so the 44% mass fraction is approximately equal to the mass of the impactor.
554 This 44% vapor fraction depends on the pressures reached in the impact, the equation of
555 state of the materials, as well as the detailed evolution of the debris in the fireball. The
556 fate of this vapor phase material is not well understood, and has been little studied.

557 Presently, $100 \mu\text{m}$ and larger sized micro-meteoroids ablate to vapor in the upper
558 atmosphere. Hunten et al. (1980), following earlier suggestions, modeled the
559 condensation of these rock vapors as they form nm-sized particles in the mesosphere and
560 stratosphere. Bardeen et al. (2008) produced modern models of their distribution based
561 on injection calculations from Kalashnikova et al. (2000). Hervig et al. (2006) and Neely
562 et al. (2011) showed that these tiny particles are observed as they deposit about 40 tons of
563 very fine grained material on Earth's surface per day. It is likely that a similar process
564 occurred after the Chicxulub impact. However, in the Chicxulub case the vaporization
565 occurred during the initial asteroid impact at Chicxulub rather than on reentry of the
566 material after the fireball rose thousands of km into space and dispersed over the globe.

567 The presence of 15-25 nm diameter, iron-rich material has been recognized in the fireball
568 layer at a variety of sites by Wdowiak et al. (2001), Verma et al. (2002), Bhandari et al.
569 (2002), Ferrow et al. (2011) and Vajda et al. (2015) among others. The nano-phase iron
570 correlates with iridium, is found worldwide, and therefore is likely a product of the
571 impact process. Unfortunately, these authors have not quantified the amount of this
572 material that is present. Berndt et al. (2011) were able to perform very high-resolution



573 chemical analyses, and also report a component of the platinum group elements that
574 arrived later than the bulk of the ejecta, and was probably the result of submicron sized
575 particles. However, they were not able to size the particles, nor quantify their abundance.

576 In Table 1 we take the injected mass of nano-particles to be 2×10^{18} g. This choice is
577 consistent with the vapor mass estimate of Johnston and Melosh (2012b). We assume an
578 initial diameter of 20 nm, following Wdowiak et al. (2001). We assume the particles are
579 initially injected over the same altitude range as the Type 2 spherules, because we
580 speculate that the small particles would not separate from the bulk of the ejecta in the
581 fireball until the ejecta entered the atmosphere and reached terminal velocity. The mass
582 injected would lead to an optical depth of particles larger than 1000 even if they
583 coagulated into the $1 \mu\text{m}$ size range. Goldin and Melosh (2009) point out that such an
584 optically thick layer of small particles left behind by the falling large spheres might also
585 be important for determining whether the infrared radiation from the atmosphere heated
586 by the Type 2 spherules is sufficient to start large-scale fires.

587 The optical properties of the nano-particles are not known. We suggest using the optical
588 properties of the small, vaporized particles currently entering the atmosphere from Hervig
589 et al. (2006). These optical constants are plotted in Figure 3. We also assume that the
590 particles have the density of CM2 asteroids, since Cr isotope ratios suggest that is the
591 composition of the K-Pg impactor (Trinquier et al., 2006). This density is 2.7 g cm^{-3} . A
592 significant fraction of the vaporized material may be from the impact site, so using an
593 asteroidal composition to determine the density is an approximation.

594

595 **2.3.2 Nano-particles from the vaporized material from a 1 km impact**

596 Johnson and Melosh (2012b) did not comment on the amount of vapor that would be
597 expected to not condense as spherules from a 1 km diameter impact. From the theory of
598 impacts, it is expected that an amount of impactor plus target that is about twice the mass
599 of the impactor would be converted into vapor from a 1 km diameter impact, just as it is
600 for a 10 km diameter impact. In Table 3 we assume that about 35% of the impactor mass
601 plus an equivalent amount of target material, would be left as vapor after spherules form.
602 We chose this mass fraction, which is lower than that for the K-Pg object, because the
603 1 km impact will have a smaller fireball, and be more confined by the atmosphere. We
604 also assume the injected particles will have a diameter of 20 nm. From simple energy
605 balance along a ballistic trajectory we would expect that the vaporized ejecta in the
606 fireball from a 1 km impact would rise about a thousand km above the Earth's surface.
607 This altitude is consistent with limited numerical calculations for large energy releases,
608 which indicate that the vertical velocity of the fireball is not significantly reduced in
609 passing through the atmosphere (Jones and Kodis, 1982). As the material reenters the
610 atmosphere, the particles will come to rest when they encounter an atmospheric mass
611 comparable to their own mass. Hence it is likely that the altitude distribution of the nano-
612 particles from the 1km impact will be the same as we have assumed for the K-Pg
613 impactor in Table 1, which is also similar to, but slightly lower in altitude than the
614 vertical distribution of micrometeorites on present day Earth as discussed by Bardeen et
615 al. (2008). It is difficult to determine precisely the area that will be covered by this
616 material as it reenters the atmosphere. If we assume that it takes about 30 min for the



617 debris to reach peak altitude and return to the Earth, and that the plume is spreading
618 horizontally at about 4 km/s then the debris would enter the atmosphere over an area of
619 about half that of the Earth. These estimates of area covered are consistent with the
620 observations of the SL-9 impact collisions with Jupiter, and the plume from the much less
621 energetic impact at Tunguska, though these are not perfect analogs (Boslough and
622 Crawford, 1997). The optical depth of the nano-particles from the 1 km diameter impact
623 averaged over the Earth is estimated for comparison with the estimates of other types of
624 particles to be relatively large, 1.5, as noted in Table 3.

625

626 **2.4 Submicron clastics**

627 **2.4.1 Submicron clastics from the Chicxulub impact**

628 Another clear component of the K-Pg debris layer is pulverized target material. This
629 clastic material was first recognized from shocked quartz grains (Bohor, 1990), but there
630 are also shocked carbonate particles from the Yucatan Peninsula in the K-Pg boundary
631 layer material (Yancy and Guillemette, 2008; Schulte et al., 2008). Because of chemical
632 alteration of much of this material in the past 65 million years it is difficult to determine
633 the mass and size distribution directly except for the shocked quartz, which is readily
634 identified. The shocked quartz grains generally are large and would not have remained
635 long in the atmosphere. However, the shocked quartz is probably not directly related to
636 the bulk of the clastics. For instance, within 4000 km of Chicxulub the shocked quartz is
637 primarily in the few mm thick fireball layer, which is distinct from the several cm or
638 thicker ejecta layer that is dominated by clastics. The shocked quartz likely came from
639 basement rock, reached higher shock pressures than the bulk of the pulverized ejecta and
640 therefore was distributed globally in the impact fireball along with the melted and
641 vaporized material from the target and impactor. The other pulverized material, in
642 contrast, came mainly from the upper portions of the target along with basement rocks
643 toward the exterior of the crater, and the fragments were distributed locally (within about
644 4000 km of Chicxulub) in the impact ejecta debris.

645

646 The submicron fraction of the clastics is of interest because particles of such size might
647 remain in the atmosphere for months or years and perturb the climate, unlike larger
648 particles that would be removed quickly by sedimentation. For instance, Pueschel et al.
649 (1994) found 3-8 months after the 1991 eruption of Mt. Pinatubo in the Philippines that
650 volcanic dust particles with a mean diameter near 1.5 μm were optically important in the
651 lower stratosphere in the Arctic.

652 The optical constants for the injected clastics are suggested from their composition. For
653 the Chicxulub impact the clastic material is largely carbonate evaporates. We suggest
654 using the optical constants of limestone from Orofino et al. (1998). Unfortunately, the
655 values need to be generated from a table of oscillator strengths. They also need to be
656 interpolated into the visible wavelength range. We suggest extending the oscillator
657 predictions into the visible range as done by Querry et al. (1978). The density of
658 limestone is in the range of 2.1-2.6 g cm^{-3} , while dolomite and anhydrite have densities
659 near 2.9 g cm^{-3} . Granite has a density near 2.6-2.8. While each of these materials
660 contribute to the clastic debris, for convenience we assume the pulverized ejecta have a



661 density of 2.7 g cm^{-3} .

662 Pope (2002) and Toon et al. (1997) used two different methods to determine the amount
663 of the submicron-clastic material from the Chicxulub impact. Unfortunately, these
664 estimates disagree by about 4 orders of magnitude, as indicated in Table 5, third row,
665 columns 1 and 2. Toon et al. (1997) used arguments based mainly on impact models, to
666 estimate that more than 10% of the mass of the distal layer ($> 7 \times 10^{17} \text{ g}$) is submicron
667 diameter clastics, which would be significant to climate. Pope (2002) estimated that the
668 clastics in the distal layer have a mass that is $< 10^{14} \text{ g}$. Pope (2002) used data on shocked
669 quartz to constrain the amount of clastics, which in principle is a better approach than
670 using estimates based on a model as in Toon et al. (1997). The amount of clastics of all
671 sizes in the Pope (2002) model (10^{16} g) is only 12-30 times larger than the clastics of all
672 sizes emitted in the relatively small 1980 Mt. St. Helens eruption. Therefore, based on
673 Pope's (2002) analysis, the submicron fraction would not be of significance to climate.
674 Below we attempt to reconcile these two approaches to better determine the amount of
675 submicron clastics.

676 **2.4.1.1 Potential errors in the Toon et al. estimate of submicron clastics**

677 Toon et al. (1997) estimated the amount of submicron **clastics** starting from analytical
678 models of the mass of material injected into the atmosphere by a 45-degree impact. They
679 estimated the mass of melt + vapor per megaton of impact energy ($\sim 0.2 \text{ Tg/Mt}$) and the
680 mass of pulverized material per megaton of impact energy (about 4.5 Tg/Mt). Assuming
681 a $1.5 \times 10^8 \text{ Mt}$ impact, these formulae suggest a melt + vapor amount of $3 \times 10^{19} \text{ g}$ ($\sim 1 \times 10^4$

682 km^3 , assuming a density of 2.7 g cm^{-3}) and a pulverized amount of $7 \times 10^{20} \text{ g}$ ($\sim 2.5 \times 10^5$
683 km^3). While sophisticated impact calculations generally agree with the amount of melt +
684 vapor, not all of it is found to reach high enough velocity to be ejected from the crater.
685 For example, Artemieva and Morgan (2009) investigated a number of impact scenarios
686 that created transient craters with diameters of 90-100 km, which they thought to be
687 consistent with the transient diameter of the Chicxulub crater. Considering those cases
688 with oblique impacts from 30-45 degrees with energies of $1.5\text{-}2 \times 10^8 \text{ Mt}$, they found that
689 the melt was in the range 2.6×10^4 to $3.8 \times 10^4 \text{ km}^3$. However, the amount that reached high
690 enough speed to be ejected from the crater was in the range 5×10^3 to $6 \times 10^3 \text{ km}^3$ (average
691 $5.6 \times 10^3 \text{ km}^3$, $1.4 \times 10^{19} \text{ g}$, about 2-10 impactor masses). On average, only about twenty
692 percent of the melt and vapor amount escapes from the crater. Therefore, Toon et al.
693 (1997) may have overestimated the amount of melt escaping from the crater by about a
694 factor of 2. It should be noted that in Artemieva and Morgan (2009) the melt exceeds the
695 mass of the distal layer, which is about $4 \times 10^{18} \text{ g}$, by about a factor of 5, because much of
696 the melt is deposited as part of the ejecta curtain and never reaches the distal region.

697 Artemieva and Morgan (2009) find that the total mass ejected from the crater is 1.3×10^4
698 km^3 ($2.9 \times 10^{19} \text{ g}$). Assuming that 90% of this material is pulverized rock their results
699 imply that Toon et al. (2007) overestimated the amount of clastic debris ejected from the
700 crater by a factor of about 25. In column 3 of Table 5 we correct the amount of
701 pulverized material to agree with the Artemieva and Morgan (2009) value of $2.9 \times 10^{19} \text{ g}$
702 of clastics escaping the crater. It is interesting to note that the clastic mass from
703 Chicxulub is only a factor of about 10 larger than the minimal estimated mass of clastics
704 ejected in the Toba volcanic eruption about 70,000 years ago (Matthews et al., 2012).



705 Another issue is the fraction of the pulverized debris that is submicron. Toon et al. (1997)
706 computed the amount of pulverized debris whose diameter is smaller than $1\ \mu\text{m}$ from size
707 distributions measured in nuclear debris clouds originating from nuclear tests that were
708 many orders of magnitude lower in energy than the K-Pg impact, and from impact crater
709 studies cited by O'Keefe and Ahrens (1982) based on grain size measurements from
710 craters. Toon et al. (1997) assume that 0.1% of the total clastic material would be
711 submicron. Pope (2002) cited studies of volcanic clouds to conclude that 1% by mass of
712 the pulverized material would be submicron.

713 Rose and Durant (2009) examined the Total Grain Size Distribution (TGSD) from a
714 number of volcanic eruptions and concluded that the amount of fine ash is related to
715 increasing explosivity of the event. The TGSD is supposed to represent the size
716 distribution as the clastics left the crater. Mt. St. Helens is the most likely of the volcanic
717 eruptions they considered to be relevant to the extreme energy release in a large impact.
718 About 2% of the total ejecta from Mt. St. Helens had a diameter smaller than $1\ \mu\text{m}$. Since
719 the erupted mass was about $3\text{-}8 \times 10^{14}$ g, the submicron mass emitted by Mt. St. Helens
720 was about $6\text{-}16 \times 10^{12}$ g. Matthews et al. (2012) considered the Toba eruption, whose
721 clastics are within an order of magnitude of those from Chicxulub. Their data shows that
722 1-2% of the mass of the clastics is in particles smaller than $1\ \mu\text{m}$ and 2-6% in clastics
723 smaller than $2.5\ \mu\text{m}$.

724 In Table 5 we use 2% of the pulverized material as a revised estimate for the fraction of
725 the clastic material that is released as submicron ejecta. This fraction is a factor of 20
726 larger than the one used in Toon et al. (1997). Hence our revised submicron mass
727 estimate for the Chicxulub impact (column 3 row 3) is very similar to the one Toon et al.
728 (2007) estimated (column 2 row 3) because, although we lowered the estimate of the
729 clastic mass exiting the crater to agree with Artemieva and Morgan (2009), we increased
730 the estimate of the fraction that is submicron.

731 A confounding issue is the amount of submicron and other clastics that escapes from the
732 near crater region and is distributed globally. A large fraction of the pulverized debris in
733 the ejecta curtain was removed within 4000 km of the impact crater (Bohor and Glass,
734 1995), and volcanic ejecta is likewise largely removed near the volcanic caldera. For
735 example, there is 4-8 cm of ash 3000 km from the Toba crater, which is not too different
736 from the thickness of the Chicxulub deposits at a similar distance from the crater. If the
737 removal occurred only by individual particle sedimentation, one could simply take the
738 mass in the smaller ranges of the size distribution and assume it spread to the rest of the
739 globe. However, it is clear from volcanic eruption data that a significant fraction of the
740 submicron debris is removed near the volcano by processes other than direct
741 sedimentation (Durant et al, 2009; Rose and Durant, 2009). These processes include
742 rainout of material from water that condenses in the volcanic plume, and also
743 agglomeration possibly enhanced by electrical charges on the particles. It is likewise
744 clear that such localized removal occurred after the K-Pg impact. Yancy and Guillemette
745 (2008) describe accretionary particles that make up a large fraction of the debris layer as
746 far as 2500 km from the Chicxulub crater. These agglomerated particles, which range in
747 size from tens to hundreds of μm , are composed mainly of particles with a radius of 1-4
748 μm . While largely composed of carbonate, the particles are enriched in sulfur.

749 One can use the size distributions from volcanic data, along with the total clastic mass



750 ejected from Chicxulub to compute the particle agglomeration, and thereby follow the
751 particles as they spread across the Earth. Such work is now being done for volcanic
752 events, for example by Folch et al. (2010). They find that they can successfully reproduce
753 mass deposited on the surface from the Mt. St. Helens eruption by including
754 agglomeration. However, such calculations for Chicxulub are difficult for several
755 reasons: the large clastic masses involved exceed the mass of the atmosphere for a
756 considerable distance from the crater, so the debris flows cannot be reproduced in
757 standard climate models; the complexity of the distribution of material in the plume with
758 some material reaching escape velocity and other parts being hurled over a substantial
759 fraction of the planet make it difficult to determine the spatial distribution of the material,
760 and some material is likely lofted well above the tops of most climate models; and the
761 presence of clastics, melt and rock vapor together with sulfur and water produces a
762 chemically complex plume.

763 Eventually it will be necessary to use detailed non-hydrostatic, multiphase plume models
764 including agglomeration to better understand the distribution of Chicxulub ejecta. In the
765 meantime for climate modeling we suggest placing the clastic mass in Table 5 (2.9×10^{19}
766 g) in a circular area with radius of 4000 km, which is 22.4% of the area of Earth. This
767 will result in a column density of 25 g cm^{-2} , or a layer thickness of about 10 cm. The
768 mass density of the atmosphere is about 1000 g cm^{-2} , so this is about a 2.5% perturbation
769 to the mass of the atmosphere. In reality the mass is concentrated near the crater as
770 shown by Hildebrand (1993). However, the observed mass density is relatively constant
771 between 1000 and 4000 km. The initial vertical distribution of this material may be very
772 complex due to density flows within several hundred km of the crater. We suggest
773 initializing models assuming an injection with an altitude independent mass mixing ratio
774 of about 2.5%. Given our suggested vertical distribution 90% of the material will
775 initially lie in the troposphere. Tropospheric material is unlikely to become globally
776 distributed even if it escapes agglomeration, because it will quickly be removed by
777 rainfall.

778 As an alternative to the complexity of modeling the loss of this material in the
779 troposphere and considering the entire size distribution, we suggest simply placing an
780 appropriate mass into the stratosphere. The values for a stratospheric injection are given
781 in the bottom row of Table 5 and the first row of Table 1. For illustration, we have
782 estimated the final optical depth assuming that 10% of the submicron material (the
783 amount placed into the stratosphere) will escape removal. For a size distribution we
784 suggest using the smaller size mode measured in the stratosphere after the Mt. St. Helens
785 eruption as summarized by Turco et al. (1983). This size distribution is log-normal (Eq.
786 1), with a mode radius of $0.5 \mu\text{m}$ and a standard deviation of 1.65. The estimated optical
787 depth of 88 is very large, even though the submicron clastic material in this estimate is
788 only about 1% of the mass of the distal layer.

789

790 **2.4.1.2 Potential errors in the Pope (2000) estimate of submicron clastics**

791 Pope (2002) determined the amount of clastics by modeling the amount of quartz in the
792 distal layer. He found that he needed an initial injection of about 5×10^{15} g of quartz to
793 match the distribution of quartz mass with distance from the impact site. It is not clear



794 how good this estimate is because, as discussed below, the removal rate of material in
795 large volcanic clouds, a possible impact analog, does not occur by individual particle
796 sedimentation, but rather by settling of agglomerates. Hence removal in the region near
797 the impact site may have been larger than Pope estimated, requiring a larger volume of
798 quartz; or the removal of clastics may be different than that of quartz. The value in
799 Artemieva and Morgan (2009) for the pulverized material ejected from the crater is 3
800 orders of magnitude larger than the estimate of Pope (2002). Most of this material is in
801 the ejecta curtain, not in the impact fireball, and so is deposited close the impact crater.
802 The shocked quartz is primarily associated with the impact fireball, so the bulk of the
803 pulverized material may not be seen in Pope's analysis.

804 Pope assumed that quartz composed 50% of all the clastic debris, so that all of the
805 clastics injected weighed about 10^{16} g. This number is about two orders of magnitude less
806 than the clastics from the Toba eruption (Matthews et al., 2012), and more than 3 orders
807 of magnitude less than the Artemieva and Morgan (2009) estimate for clastics from the
808 Chicxulub impact.

809 The assumption by Pope (2002) that quartz is 50% of all the clastics is likely in error.
810 There is no reason to think there is much quartz in the upper layers of sediment at the
811 Chicxulub site. In the stratigraphic columns shown by Ward et al. (1995) the pre-impact
812 sediments at Chicxulub consist of approximately 3 km of Mesozoic carbonates and
813 evaporites with ~3-4% shale and sandstone. Therefore, it is more likely the quartz
814 originates from the basement rocks. There is also not a strong connection between the
815 physical processes that distributed the quartz (the impact fireball, with high ejection
816 velocity), and those that distributed the pulverized material (the ejecta curtain with low
817 velocity).

818 It is possible that the quartz to clastics ratio is determined by the ratio of quartz to total
819 debris in the samples closest to Chicxulub, since these may have suffered the least removal
820 by sedimentation. Pope suggests these intermediate distance layers contain about 1%
821 quartz, but only considers the fireball layer, which is less than 10% of the total ejecta layer
822 within 1000 km of the crater. The remainder of the intermediate distance layer contains
823 little quartz, so the clastics could be more than 1000 times the mass of the quartz. It is not
824 clear that 1000 is an upper limit to the ratio of clastics to quartz because the quartz and
825 pulverized material move along different paths in the debris cloud. If we accept this ratio
826 of 1000 for the ratio of clastics to quartz, the mass of clastics from Pope's analysis would
827 be 5×10^{18} g, which is within a factor of 6 of the Artemieva and Morgan (2009) value. If 1%
828 of this mass is submicron then 5×10^{16} g of submicron clastics would have been injected into
829 the upper atmosphere.

830 **2.4.1.3 Reconciliation of Pope (2000) and Toon et al. (1997) estimates of submicron** 831 **clastics**

832 Table 5 shows that the new estimate of submicron mass following the procedure of Toon
833 et al. (1997) agrees with the new estimate following the procedure of Pope (2002). The
834 new estimate is about 12 times less than the Toon et al. (1997) value mainly because
835 Toon et al. (1997) did not consider that most of the pulverized mass would not be ejected
836 from the crater. The new application of the Pope (2002) approach is about 500 times
837 larger than the one used by Pope (2002), mainly because we have assumed the ratio of



838 quartz to clastics is about 1000, rather than 1 as assumed by Pope (2002). Despite the,
839 perhaps coincidental, agreement of these two estimates, there is substantial uncertainty in
840 the true mass of submicron clastic particles in the K-Pg distal layer. Observations of the
841 submicron material in the distal layer are needed.

842

843 **2.4.2 Submicron pulverized rock from a 1 km diameter impactor**

844 In order to determine the properties of the pulverized ejecta from a 1 km impactor, we
845 use the pulverized mass injection per Tg of impact energy from Toon et al. (1997), but
846 reduce it by the factor of 25 discussed earlier to account for the fraction of the clastic
847 mass with enough velocity to escape the crater. This procedure yields a clastic mass of
848 1.3×10^{16} g. For reference, the volume of clastics from the eruption of Mt. Tambora in
849 1815 is estimated to have been about 150 km^3 , which is a mass of about 3×10^{17} g. Hence
850 the Tambora eruption likely surpasses the clastics from the hypothetical 1 km diameter
851 impactor by more than a factor of 10. The same size distribution for the clastics is
852 recommended for the 1 km impact and the Chicxulub impact, since it seems to hold for a
853 range of volcanic events from Mt. St. Helens to Toba, which span the 1 km diameter
854 impactor in terms of clastics. We also suggest that the mass be initially mixed uniformly
855 in the vertical above the tropopause. According to Stothers (1984) the Tambora clastics
856 were deposited in layers that are centimeters in thickness at distances 500 km from the
857 volcano. Accounting for the drift of the ash downwind, the area of significant ash fall
858 was about $4.5 \times 10^5 \text{ km}^2$. If this same area is used for the initial injection of the clastics for
859 the 1 km impact, then the column mass concentration is about 8.7 g cm^{-2} , which in turn is
860 slightly less than 1% of the atmospheric column mass. The estimated optical depth of the
861 clastics in Table 3 is about 25% of the optical depth from nano-particles originating from
862 vaporized rock. Given that these materials are much less absorbing than soot, and lower
863 in optical depth than nano-particles they can probably be neglected in estimates of the
864 climate changes due to a 1 km diameter impact on land.

865 **3. Gas injections**

866 There are a large number of gases that might be injected into the atmosphere after an
867 impact and might be important to atmospheric chemistry, climate, or both. These can
868 originate from the impactor itself, from ocean or ground water, or from the target
869 sediments. They may also originate in response to environmental perturbations, such as
870 wildfires, or atmospheric heating from the impact fireball and ejecta. Various estimates
871 have been made for each of these sources. However, clear evidence from the distal layer
872 is not available for any gases of potential interest. Some gases, such as carbon dioxide,
873 would have stayed in the gas phase rather than condensing into particulate form. Other
874 gases, such as those containing sulfur, may have reacted on the particles composing the
875 distal layer, or formed independent particles. In either case sulfur is so common in the
876 environment it is difficult to detect an injection. For these reasons all the gas phase
877 injections are uncertain. Below, we first discuss the chemical content of each of the
878 potential sources of gases, and then we discuss the likely amounts of each material
879 injected following an impact. Relevant ambient abundances are given in Table 2 and 4
880 along with estimated injections for Chicxulub and 1 km impacts. The ambient masses are
881 given to assist the reader in understanding the magnitudes of the injections. Generally



882 ambient concentrations are given in the literature in terms of the mixing ratio. To
883 compute the masses we assume the ambient mixing ratios are constant over the whole
884 atmosphere, or the stratosphere. We then convert the volume mixing ratio to the mass
885 mixing ratio using the molecular weight and then multiply by the mass of the atmosphere
886 above either the surface, or tropopause to obtain the total mass of the gas. The ambient
887 abundances assume the current stratospheric mixing ratio of Cl is 3.7 ppbv (Nassar et al.,
888 2006), Br is 21.5 pptv (Dorf et al., 2006), inorganic I is 0.1pptv (upper limit from Bosch
889 et al. 2003), CO₂ is about 395 ppmv, and methane is about 1.8 ppbv. Stratospheric S,
890 taken from the Pinatubo volcanic eruption, is about 10 Tg (Guo et al., 2004), Reactive
891 nitrogen, NO_x, in the stratosphere is difficult to quantify simply. Instead we compare
892 with the ambient abundance of N₂O in the stratosphere, about 2x10¹⁴ g N. N₂O is a major
893 source of NO_x.

894

895 **3.1 Impactor**

896 **3.1.1 Composition of the impactor**

897 Kring et al. (1996) summarized the S, C, and water contents of a large number of types of
898 asteroids. Trinquier et al. (2006) found from chromium isotopes that the Chicxulub
899 impactor was most likely a carbonaceous chondrite of CM2 type. Such asteroids have
900 3.1wt % S, 1.98 wt% C, 11.9 wt% water, and a density of 2.71 g cm⁻³. Over the range of
901 chondrites, which constitute 85% of meteorite falls, S varies from 1.57 to 5.67 wt%, C
902 from 0.04 to 3.2 wt %, and water from 0.2 to 16.9 wt %. Kallemeyn and Watson (1981)
903 report that by mass CM carbonaceous chondrites contain about 4ppm Br. Goles et al
904 (1967) report that Cl ranges from 190-840 ppmm of carbonaceous chondrites, Br ranges
905 from 0.25 to 5.1 ppmm, and Iodine ranges from 170 to 480 ppbm. Table 6 summarizes
906 the composition of asteroids using values for CM2 type carbonaceous chondrites from
907 Kring et al. (1996) for S, C, and water, and for the Mighei (the CM2 type example) from
908 Goles et al. (1967) for Cl, Br and I.

909 **3.1.2 Gases from the impactor**

910 Tables 2 and 4 indicate the direct contributions from 1 and 10 km impactors of a number
911 of chemicals, as discussed further below. We assume that the entire 10 km or 1 km
912 diameter impactor melted or vaporized so that all of the gases are released. For the 10
913 km impactor these gases would have been distributed globally in the hot plume along
914 with the melt spherules within hours. They would reenter with the same vertical
915 distribution as the Type 2 spherules. For the 1 km diameter impactor, the initial injection
916 may have only covered half the Earth, with global distribution over days via wind, after
917 reentry into the upper atmosphere.

918 We further assume that the vapors under consideration do not react with the hot mineral
919 grains either in the plume or in the hot layer at the reentry site. In fact, given the large
920 particle surface areas in the atmosphere over the globe it is possible that there was a
921 significant transfer of material from the gas phase to the surfaces of the mineral grains in
922 a short period of time.

923 As pointed out by Kring et al. (1996) and Toon et al. (1997) the S in a 10 km diameter
924 impactor would exceed that from the Mt. Pinatubo volcanic injection by a factor above



925 1000. Even a 1 km diameter carbonaceous chondrite could deliver several times as much
926 sulfur to the atmosphere as did the Mt. Pinatubo eruption in 1991. Stratospheric water
927 could be enhanced by a factor of more than 100 from the water in a 10 km impactor. Cl
928 could be enhanced by factors above 500, Br by almost 500, and I by more than 50,000.
929 However, there is not enough C in a 10 km asteroid to affect the global carbon cycle
930 significantly.

931 Many investigators have pointed to sulfate as an important aerosol following the
932 Chicxulub impact. Tables 1 and 3 compare the mass of sulfur from the impactor with the
933 mass of the spherules and nano-particles. The optical depth, which controls the climate
934 change following the impact, and the particle surface area, which likely controls
935 chemistry, are approximately linear with the mass. In our estimates, the sulfate coming
936 directly from the asteroid could have a large optical depth assuming it was not removed
937 on the spherules, or large clastics.

938

939 **3.2 Seawater**

940 **3.2.1 Composition and depth of seawater**

941 The composition of seawater is given in Table 6 (Millero et al., 2008). It is thought that
942 injections of water into the upper atmosphere will lead to droplet evaporation, with small
943 crystals of salt left behind. If liquid water is left after a massive injection of water, the
944 droplets will likely freeze leaving salt behind as particles embedded in ice crystals.
945 Vaporization of water during the impact may leave behind salt crystals, or the salts may
946 decompose into their components. As discussed by Birks et al. (2007), complex
947 simulations are needed to determine how much material is freed from the salt particles to
948 enter the gas phase where it might destroy ozone. In Table 2 and 4 we list the total
949 amounts of several interesting chemicals that might be inserted into the stratosphere.
950 However, all of them except water vapor are likely to be in the form of a particulate until
951 photochemical reactions liberate them.

952 A significant uncertainty related to any oceanic contribution to atmospheric composition
953 is the depth of the ocean in relation to the size of the impactor, and the water content of
954 sediments at the crater site. The depth of the ocean at the time of the impact is not known.
955 Many investigators have referred to it as a shallow sea. However, Gulick et al. (2008)
956 estimates that the water depth averaged over the impact site was 650 m, which is
957 considerably deeper than earlier estimates. We use a water depth of 650 m in Table 2 to
958 estimate the amounts of material injected by Chicxulub. A 1 km diameter impactor is
959 smaller than the average depth of the world oceans, which is about 3.7 km.

960 **3.2.2 Gases from Seawater-Chicxulub**

961 For the Chicxulub impact, Pope (1997) assumed that the 650 m depth of seawater within
962 the diameter of the impactor (10 km) will be vaporized, follow the path of the Type 2
963 spherules, and reenter the atmosphere globally. In Table 2 we compute the water
964 vaporized following the equations in Toon et al. (1997). These equations, assuming an
965 impact velocity of 20 km s^{-1} , led to an order of magnitude greater injection of water than
966 using Pope's estimate. The vaporized water is 0.4 times the impactor mass. During the
967 vaporization of the seawater we assume the water will be present as water vapor, and that



968 the materials in the water will be released as vapors. Some of these materials likely
969 would react quickly with the hot minerals in the fireball or later with the hot minerals in
970 the reentry layer.

971 It is also likely that a considerable amount of water was splashed into the upper
972 atmosphere. Ahrens and O'Keefe (1983) estimated that the water splashed above the
973 tropopause from a 10 km diameter impact into a 5 km deep ocean would be 30 times the
974 mass of the impactor. We assume that the amount of water splashed above the tropopause
975 will scale linearly with the depth of the ocean. Therefore, about 4 times the impactor
976 mass of water may have been splashed into the upper atmosphere. Much of this water
977 may immediately condense and rainout, as discussed in Toon et al. (1997). However,
978 some of the dissolved salts may be released if some of the water evaporates. The
979 assumed injection of gases, and particulates that might become gases, from the ocean is
980 summarized in Table 2 for the Chicxulub impact.

981 **3.2.3 Gases from Seawater-1 km asteroid**

982 No seawater is injected by the 1 km diameter asteroid impact on land. If a comet hit the
983 land there would be a water injection.

984 Pierazzo et al. (2010) estimated that 43 Tg of water would be injected above 15 km by a
985 1 km asteroid impact into the deep ocean. Of this water, 25% is in the form of vapor and
986 75% in the form of liquid water. In their modeling the water was assumed to be
987 distributed with a uniform mixing ratio from the tropopause to the model top. It was also
988 spread uniformly over an area 6200x6200 km in latitude and longitude. Using the
989 equations in Toon et al. (1997) for the vaporized water produces a value which is 60%
990 of the vaporized water from the detailed modeling used in Pierazzo et al. (2010). Given
991 these water injections we use the composition of sea water to determine the injections of
992 the various species. Pierazzo et al. (2010) estimate injections of Cl and Br that are more
993 than an order of magnitude smaller than ours because they consider the amounts that have
994 been converted into gas phase Cl and Br by photochemical reactions in the atmosphere,
995 while we estimate the total injections, which initially are likely to be in the particulate
996 phase.

997

998 **3.3 Impact Site**

999 **3.3.1 Composition of the impact site**

1000 The sea floor at the Chicxulub impact site, like the modern Yucatan, contained abundant
1001 carbonate and sulfate rich deposits. Ward et al. (1995) conclude that 2.5-3 km of
1002 sedimentary rock were present at Chicxulub, composed of 35-40% dolomite, 25-30%
1003 limestone, 25-30% anhydrite, and 3-4% sandstone and shale. The dolomite and
1004 limestone are no doubt porous. Pope et al. (1997) estimate the carbonates in the Yucatan
1005 have a porosity of 20%. The pores would have been filled by seawater since the
1006 sediments were submerged. This ground water produces an equivalent water depth of
1007 about 400 m. The carbon content of limestone is 12% by weight, and of dolomite 15%
1008 by weight. The sulfur content of anhydrite is 23.5% by weight. To our knowledge, trace
1009 species such as Br, Cl, and I have not been reported for these sedimentary rocks, but
1010 would be present in the seawater in the pores.



1011 **3.3.2 Gases from the impact site**

1012 For the 10 km Chicxulub impact we follow Pope et al. (1997) for the abundances of S
1013 and C assuming 30% anhydrite, 30% limestone and 40% dolomite. The composition of
1014 the impact site is given in Table 6. We ignored species other than S and C that might be
1015 in the target material. It is difficult to follow the target debris since some of it is
1016 vaporized, and some melted. We follow Pope (1997) and assume that the upper 3 km of
1017 the target is vaporized within the diameter of the impactor. The gases within this volume
1018 of vaporized material are assumed to be released, and to follow the trajectories of the
1019 Type 2 spherules. Pope et al. (1997) estimated the amount of material that would be
1020 degassed from target material that was melted or crushed in a large impact. We use the
1021 values from Table 3 of Pope et al. (1997) for out of footprint vapors, in our Table 2 for
1022 the degassed impact site emissions. We also assume that the granite underlying the
1023 impact site does not contribute.

1024 The source gases from a 1 km land impact would depend on the composition of the
1025 impact site, so we do not list values in Table 4. We assume nothing would be liberated
1026 from the sea floor in a 1 km impact in the deep ocean.

1027

1028 **3.4 Fires**

1029 **3.4.1 Composition of Smoke**

1030 It is well known that forest fires emit a wide variety of vapors into the atmosphere.
1031 Andreae and Merlet (2001) provide emission ratios (g of material emitted per g of dry
1032 biomass burned) for many vapors expected to be important in the atmosphere as listed in
1033 Table 6. As discussed in section 2.2.1, the soot emission may have been enhanced
1034 relative to wildfire estimates by Andreae and Merlet (2001) after the Chicxulub impact
1035 because the impact-generated fires were mass fires. We do not consider any
1036 enhancements of the gas phase emission ratios, but they may also be impacted by fire
1037 intensity or the types of plants making up the biomass.

1038

1039 **3.4.2 Gases from Fires**

1040 In Tables 2 and 4 we computed the burned mass from Chicxulub assuming that 1.5 g cm^{-2}
1041 of dry biomass burns over the entire land surface area of the Earth, and then used the
1042 emission factors from Andreae and Merlet (2001) to obtain the gas phase emissions. For a
1043 1 km impact we assume the area burned is $4.1 \times 10^4 \text{ km}^2$ (Toon et al., 1997), and the dry
1044 biomass is 2.25 g C cm^{-2} . We then used the emission ratios from Andreae and Merlet
1045 (2001) to compute the gas phase emissions. Comparing the gas phase emissions from
1046 fires in Tables 2 and 4 with ambient values indicates that there would be large
1047 perturbations for all gases for the 10 km diameter impact. Only iodine is significantly
1048 perturbed for the 1 km impact. For the gas phase emissions we suggest using the same
1049 vertical profile as suggested for soot earlier. The emissions would only occur over the
1050 region near the impact site for the 1 km impact.

1051 **3.5 Gases generated by atmospheric heating**



1052 The energy deposited in the upper atmosphere by the initial entry of the bolide, as well as
1053 by the rising fireball, may have converted some N_2 to NO_x . Early studies suggested that
1054 a large fraction of the impact energy would be put into the lower atmosphere, which in
1055 turn led to suggestions that a large amount of nitrogen oxides would be produced from
1056 the heated air. However, it is now understood that most of the energy release from an
1057 impact to the atmosphere will occur at high altitude from reentry of spherules and other
1058 debris. Toon et al. (1997) reviewed the various ways in which NO_x might be generated
1059 following an impact, largely following Zahnle (1990). They concluded that 3×10^{16} g of
1060 NO might be produced from the atmosphere for a 10 km diameter impact with about half
1061 coming from the plume at the impact site, and half from the reentry of material across the
1062 Earth. We have recorded this value in Table 2. For comparison, Parkos et al. (2015)
1063 conducted detailed evaluations of the NO_x produced by the infalling spherules and
1064 concluded the spherules could produce 1.5×10^{14} moles of NO_x (3×10^{15} g if the NO_x is in
1065 the form of NO) which they further concluded was not sufficient to acidify ocean surface
1066 waters. In Table 2 we use the Toon et al. (1997) injection of NO since it includes both
1067 source mechanisms. From Zahnle et al. (1990) a 1 km land impact might produce $0.6 \times$
1068 10^{14} g of NO, largely in the hot plume at the impact site. This value is entered in Table 4.
1069 For comparison, we note that Pierazzo et al. (2010) suggested that the mass of NO
1070 produced by a 1 km ocean impact is about 0.39×10^{14} g.

1071

1072 **3.6 Discussion of gas injections**

1073 Some of the gas phase sources just discussed are easy to apply to an impact. For
1074 example, the emissions from fires simply depend on the area burned, the fuel loading and
1075 the emission factors.

1076 Other sources of gases are more difficult to evaluate. Since we have no measurements for
1077 large impacts, the form of emission can be uncertain. For example, sulfur could be
1078 injected as SO_2 or SO_3 . Another difficulty that comes in understanding the contribution
1079 of target material to gases, such as SO_2 , is the pressure needed to vaporize the material.
1080 Pope (1997), for example, adopted pressures above 70 GPa to vaporize carbonate, 100
1081 GPa for complete vaporization of anhydrite, and 10 GPa for water vaporization from
1082 pores. These vaporization pressures are higher than suggested by early researchers,
1083 leading to lower amounts of target vaporized. Pierazzo et al. (2003) redid the impact
1084 calculations and also estimated the amounts of materials that might be released, which are
1085 close to those estimated by Pope (1997). The altitude distribution of the ejecta varies
1086 with the source of the material. Finally the chemical form of the emission varies with
1087 thermochemistry in the ejecta plume or fireball, and interactions with hot mineral
1088 surfaces, and for some materials exposure to high temperature on reentry.

1089 Tables 2 and 4 summarize our choices for the injections of the various gases. For each
1090 type of source we also specify the altitude of the expected injection, using a reference to
1091 Table 1 and 2 for the particle injections. We assume all of the impactor mass entered the
1092 rising fireball, so it would be injected near 60 km altitude along with the spherules. In
1093 some cases, for example for the degassed target material and for splashed seawater, we
1094 consider the material to have been uniformly mixed above the tropopause. For materials
1095 coming from fires we assume the same vertical injection as for soot.



1096 As has been pointed out many times (Kring, 1996; Toon et al., 1997; Pope, 1997;
1097 Pierazzo et al., 2003) the sulfur injection from a 10 km impactor might be thousands of
1098 times greater than that from the Pinatubo eruption, and also was likely larger than the
1099 injection from the massive Toba eruption by a factor between 10 and 100. Our sulfur
1100 injection from the target material is about half that of Pope's (1997) estimate of 10^{17} g and
1101 slightly less than Pierazzo et al's (2003) estimate for a 15 km diameter impactor of $7.6 \times$
1102 10^{16} g. Our sulfur injection from the asteroid itself is within the range suggested by Pope
1103 (1997) of $2.7\text{-}5.9 \times 10^{16}$ g. Interestingly, the sulfur injection we estimate for Chicxulub is
1104 about 10 times greater than the yearly emission estimated by Schmidt et al. (2015) for a
1105 large flood basalt from the Deccan traps. Of course, the flood basalt might continue for a
1106 decade or more, bringing the total sulfur emission close to that from the Chicxulub
1107 impact. Table 4 suggests that the sulfur injection from a 1 km impact would be several
1108 times greater than that from the Pinatubo eruption, but that would be only a modest
1109 injection relative to historical volcanic eruptions. In Table 1 and Table 3 we assume the
1110 injected sulfur gas is converted into sulfate. If so it would yield a large optical depth for
1111 the Chicxulub impact. However, for both the 1 km and Chicxulub impacts, the sulfur
1112 injection, if converted to sulfate, would be an order or magnitude less massive than the
1113 nano-particles. Therefore, the sulfate would be an order of magnitude less important
1114 optically than the nano-particles. While it might exceed the soot mass slightly, soot is
1115 much more important optically than sulfate, which is transparent at visible wavelengths.
1116 Therefore, the sulfate in our model is of relatively little importance optically, unless the
1117 sulfur remains in the air after the other particles are removed.

1118 Our estimated C injection (in the form of CO_2) is dominated by emissions from forest
1119 fires. We have the same emission from the impactor as Pope (1997), but we have less
1120 than half the emission from the target material as Pope (1997) or Pierazzo et al. (2003).
1121 All these studies suggest a small impact perturbation relative to the CO_2 65 million years
1122 ago, which was several times larger than now.

1123 The water vapor injections in Tables 2 and 4 are very large compared with ambient
1124 values in the stratosphere. However, most of the water is from fires, and half will be
1125 injected into the troposphere where it will be quickly removed. The water from the
1126 impactor and target is modest, about 1 cm as a global average depth of rain. The typical
1127 rainfall averaged over the current Earth is about 3 mm day^{-1} . The emissions from the
1128 impactor and from vaporized seawater, both of which would have been injected globally
1129 at the same altitudes as the Type 2 spherules, are capable of saturating the entire ambient
1130 stratosphere. Our water injection is similar to that estimated by Pope (1997), and Pierazzo
1131 et al. (2003). While the water vapor has been largely ignored in previous work on the
1132 Chicxulub impact, it has the ability to alter the thermal balance of the stratosphere by
1133 emitting and absorbing infrared light. Water vapor may have been a factor in the
1134 radiation of thermal energy to the surface during the first few hours after the K-Pg
1135 impact, since Goldin and Melosh (2009) sought an infrared absorber to prevent radiation
1136 from escaping from the top of the atmosphere. Some of the particles in the stratosphere
1137 might be removed by precipitation, but the mass of water injected is comparable to the
1138 mass of the nano-particles and spherules. Therefore, removal by precipitation is probably
1139 not significant since if the water condenses on all the particles it will add only a small
1140 mass, and increase the fall rate only slightly, while if water condenses on only a subset of



1141 the particles it will remove only a subset. The water injection by the 1 km diameter
1142 impact on land is about 15% of the ambient water, but might still lead to some significant
1143 perturbations if it is injected into the upper stratosphere. The 1 km impact in the deep
1144 ocean could inject about 40 times the ambient water into the stratosphere (Pierazzo et al.,
1145 2010), and water should be considered in simulations of such impacts.

1146 For the 10 km diameter impactor, there are injections of Cl, Br, and I that exceed the
1147 ambient values by orders of magnitude. There are significant sources for all three
1148 halogens from fires, the impactor and seawater, so it seems inescapable that large
1149 injections would have occurred. The injections of NO_x from fires, and from heating the
1150 atmosphere are also very large compared with ambient values. For instance, Table 2
1151 shows the NO_x injections are one to two orders of magnitude larger than the stratospheric
1152 burden of N₂O, the principle source of NO_x. For the 1 km diameter land impact only the
1153 injections of I and NO_x appear large enough to perturb the chemistry of the stratosphere.
1154 However, as discussed by Pierazzo et al. (2010) significant Cl and Br injections could
1155 occur for a 1 km impact in the ocean. Seawater injections of Cl, Br, I, and S are
1156 complicated because the salts may be injected in particulate form.

1157

1158 **4. Implications for climate, atmospheric chemistry and numerical modeling, and** 1159 **suggestions for future data analysis**

1160 Since the discovery of the K-Pg impact by Alvarez et al. (1980), many papers have
1161 speculated on which of the many possible effects of the impact on the environment could
1162 have caused the mass extinction. It has become fashionable to claim that one or another
1163 effect is dominant. However, it is quite likely that several effects overlapped, each of
1164 which might have been devastating to a particular species or ecosystem, but which
1165 together made survival very difficult for a broad range of species distributed over the
1166 globe. Here we summarize the environmental perturbations we find likely. However,
1167 there are many uncertainties, and additional data are needed. We outline the data that
1168 would be useful to obtain from the geologic record, and summarize it in Table 7. Also,
1169 models have barely scratched the surface of what is possible in better understanding of
1170 the post impact environment. We summarize the types of modeling work that would be
1171 interesting to pursue. We extend these ideas to smaller impacts since more than 50
1172 impacts of kilometer-sized objects may have occurred since the extinction of the
1173 dinosaurs.

1174 Table 1, shows that spherules, soot, nano-particles, submicron clastics, and sulfates each
1175 may have had very large optical depths. An optical depth greater than unity could have
1176 serious consequences for the environment if maintained for very long. Each of these
1177 materials was likely present in the atmosphere, so they may have interacted.

1178 The spherules are unlikely to have changed climate directly because they would have
1179 been removed quickly from the atmosphere by sedimentation due to their large size.
1180 However, these particles, together with the other impact debris with significant mass,
1181 likely heated the upper atmosphere to temperatures between 1000 and 2000K. The high
1182 temperature upper atmosphere would then have irradiated the surface with near infrared
1183 radiation, causing forest fires. Wolbach et al. (1985) first recognized that the global biota
1184 likely burned after the impact, and Melosh et al. (1990) identified the mechanism for



1185 starting the fires. The recent work by Goldin and Melosh (2009) identified some
1186 complexities in the ignition mechanisms that need further work to be understood. They
1187 pointed out that the light might be blocked by the large spherules falling below the heated
1188 atmospheric layer. However, this is a complex problem since water vapor, and vaporized
1189 impactor would have been present to block radiation escaping to space. Also convection
1190 should occur in such a strongly heated layer, which would act to retard the fall of the
1191 particles as it does for hailstones in tropospheric convection. These issues all deserve
1192 further study with suitable models. Furthermore, evidence for the nano-particles should
1193 be sought as discussed further below.

1194 Robertson et al. (2004) argued that large dinosaurs and other unsheltered animals could
1195 have been killed immediately by the radiation from the sky and the subsequent fires.
1196 However, it is possible there were refugia on the land, either in regions where spherules
1197 did not reenter the atmosphere, as suggested by Kring and Durda (2002) as well as
1198 Morgan et al. (2013), or in regions that happened to have heavy cloud cover which may
1199 have blocked the radiation. To better understand the possibility of refugia, more
1200 complete evidence for the global distribution of spherules would help resolve their
1201 possible non-uniform deposition, as suggested in Table 7. It is known that iridium was
1202 perturbed worldwide following the K-Pg impact. Although iridium concentrations are
1203 spatially variable for a number of reasons, they are basically homogenous over the Earth
1204 and do not fall off with distance from the impact site, or at high latitudes. Similar data on
1205 spherules would be useful to determine if the spherules were injected everywhere, or in
1206 special places. Numerical values of the spherule concentrations and size distributions to
1207 augment the values noted by Smit (1999) would also be of value, as noted in Table 7.
1208 Models of the transmission of the light from the hot debris layer above 60 km through
1209 dense water clouds and the response of the clouds to the heating would be also useful. It
1210 has long been recognized that intense thermal radiation and fires could not have been the
1211 only extinction mechanisms at work, since the mass extinctions in the oceans could not
1212 have occurred in this way, but instead were likely due to the low light levels preventing
1213 photosynthesis (Milne and McKay, 1982; Toon et al., 1982; Pollack et al., 1983; Toon et
1214 al., 1996; Robertson, et al., 2013b). The low light levels would have been caused by the
1215 high optical depths of the soot and nano-particles that remained suspended in the air for a
1216 year or more after the impact.

1217 We know from the work of Wolbach et al. (1985; 1988; 1990; 2003) that there is
1218 abundant soot in the K-Pg distal layer. It is highly likely that the soot originated from
1219 wildfires (Robertson et al., 2013a), but its origin is of secondary concern for climate. The
1220 widespread distribution of the soot in the layer, and the small size of the particles indicate
1221 this material was almost certainly global in extent. Wolbach et al. (1988) show that soot
1222 and iridium are tightly correlated across the K-Pg distal layer. The soot and iridium in
1223 the distal layer must have been deposited within a few years of the impact, since small
1224 particles will not stay in the air much longer. Therefore, any fires must have been within
1225 a year or two of the impact. As noted in Table 7, further examination of the distributions
1226 of soot, iridium and spherules might clarify how long these materials remained in the
1227 atmosphere, which is expected to be days for the spherules, and a few years for the soot
1228 and iridium on small particles. Once in the water column, spherules would fall to the
1229 bottom in days or weeks. However, in the absence of fecal pellets formed by plankton



1230 around the soot, it would take decades for soot to reach the ocean depths by falling.
1231 Currents would likely carry the soot down rather than gravity.

1232 The amount of soot in the K-Pg distal layer would produce a very high optical depth
1233 when it was in the atmosphere. The transmission of light depends not only on the optical
1234 depth, but also on the single scattering albedo of the particles. The single scattering
1235 albedo measures the fraction of the light that is scattered, or absorbed. Scattering light,
1236 which occurs from sulfates that absorb sunlight only weakly, is not nearly as effective in
1237 changing climate as absorbing light.

1238 As discussed by Toon et al. (1997), soot with an optical depth of 100 would prevent any
1239 sunlight from reaching the surface—it would be pitch black. No climate simulations of
1240 such large soot optical depths have ever been conducted. However, there have been
1241 simulations for optical depths in the range of 0.05-1, which show temperatures dropping
1242 to ice age conditions within days, precipitation falling to 50% of normal, and the ozone
1243 layer being destroyed as discussed further below (Robock et al., 2007a,b; Mills et al.,
1244 2008, 2014). There are a number of complexities inherent in climate calculations for soot.
1245 For example, it is important to know how long the soot remained in the atmosphere in
1246 order to determine how long photosynthesis may have been retarded in the oceans. The
1247 lifetime of the soot in turn may depend on the size of the soot particles, their shape, the
1248 amount of rainfall in the lower atmosphere, and the amount of sunlight reaching the soot.
1249 The amount of sunlight reaching the soot matters because heating the soot also heats the
1250 surrounding air, causing it to rise and loft the soot to high altitudes, where it is protected
1251 from rainout (Malone et al. 1985; Robock et al. 2007a,b). These issues can be considered
1252 in modern climate models.

1253 Much of the vaporized impactor and target material is thought to have re-condensed to
1254 250 μm -sized spherules (O'Keefe and Ahrens, 1982; Johnson and Melosh, 2012b), which
1255 are observed, but a significant fraction may have remained as nanometer sized grains
1256 (Johnson and Melosh, 2012b). Iron-rich, nano-phase material with a diameter of 15-25
1257 nm has been identified in the fireball layer at a variety of sites by Wdowiak et al. (2001),
1258 Verma et al., (2002), Bhandari et al. (2002), Ferrow et al. (2011) and Vajda et al. (2015)
1259 among others. However, the abundance of this nano-phase material is not yet constrained
1260 by observations. As noted in Table 7, it is important to quantify the abundance of this
1261 nano-phase material, and to confirm that it is the remnant of the vaporized target and
1262 impactor. If the estimate of Johnson and Melosh (2012b) of its abundance is roughly
1263 correct then, given the optical depth estimate in Table 1 and its input location in the upper
1264 atmosphere above the soot generated by forest fires, this nano-phase material would be
1265 the dominant source of opacity for changing the climate, and would also greatly affect the
1266 amount of radiation emitted to the surface that could start wildfires in the hours following
1267 the impact. The material contains iron, so it is likely to have been a good absorber of
1268 sunlight. Alternatively, this material might have attached itself to the large spheres and
1269 been quickly removed, though this seems unlikely since the large spheres would separate
1270 gravitationally from the smaller material within hours. No one has yet considered the
1271 effect of this nano-phase material, which is distinct from the clastics envisioned by Toon
1272 et al. (1997) and Pope (2002), on the environment after the K-Pg impact.

1273 The most massive part of the ejecta from the K-Pg crater consisted of clastics: crushed
1274 and pulverized material. Much of this material fell relatively close to the crater, though



1275 significant amounts were emplaced as far a 4000 km from Chicxulub. For comparison the
1276 Toba volcanic eruption about 70,000 years ago is estimated to have released more than
1277 2×10^{18} g of clastics (Matthews et al., 2012), a factor of about 15 less than our estimate for
1278 the Chicxulub impact in Table 1, but more than 200 times greater than the upper limit
1279 previously estimate by Pope (1997) for the clastics generated by Chicxulub.

1280 The Toba eruption may have had a significant impact on the climate, as discussed further
1281 below; however, the magnitude of the effect is controversial. Alvarez et al. (1980), as
1282 well as Toon et al. (1982) and Pollack et al. (1983), thought that the K-Pg layer was
1283 dominated by submicron clastics that caused major loss of sunlight at the surface and
1284 consequently very low temperatures. However, while we don't know the fraction of the
1285 layer composed of submicron clastics, it is clear that the layer is both thinner than thought
1286 in the years just after its discovery and also dominated by other parts of the impact debris
1287 such as the spherules and the nano-particles. It would be very useful to measure the
1288 amount of submicron clastics in the K-Pg distal layer. Possibly, as suggested in Table 7,
1289 one could start by identifying the amount of submicron quartz in the layer by searching
1290 for small shocked quartz grains. Toon et al. (1997), and Pope (2002) used two differing
1291 indirect approaches to quantify the submicron clastics, and came up with answers that
1292 differ by a factor of about 10^4 . Here we attempted to reconcile these approaches, with the
1293 result shown in Table 1 yielding a significant optical depth. Although the submicron
1294 clastics by themselves would have produced extreme climate changes if they were as
1295 abundant as we estimate, they would have been less important than the soot, and the
1296 nano-particles given our estimates here. The submicron clastics may have been injected
1297 higher than the soot, but lower than the nano-particles on average. Climate calculations
1298 involving all these materials are needed to understand how they may have interacted in
1299 the atmosphere.

1300 The final particulates with large optical depths in Table 1 are sulfates. Pope et al. (1997),
1301 Pierazzo et al. (2003) and others have advocated for the importance of these particles in
1302 recent years. Unfortunately, sulfates in the K-Pg layer have not been traced
1303 unambiguously to the impact, because sulfur is so common in the environment. Possibly
1304 sulfur isotopic studies could distinguish the sulfur in the impactor from sulfur in the
1305 terrestrial environment, but we are not aware of such studies. While there is little doubt
1306 that large amounts of sulfur were present in the target material and in the asteroid, it is
1307 possible that much of it reacted with the hot rock in the impact plume, or the atmospheric
1308 layer heated by re-entering material. Sulfur is present in impact melt spherules and in
1309 carbonaceous clastics, so not all of it was released to the gas phase. Given the large
1310 opacity of the numerous types of particles in the atmosphere, photochemical reactions
1311 would have been inhibited, which would retard the conversion of sulfur dioxide gas into
1312 sulfate particles. It is possible that measurements of the sulfur mass independent
1313 fractionation (MIF) could reveal whether the sulfur quickly reacted with rocks, which
1314 should yield a MIF of zero, or if the sulfur slowly converted to sulfate, which might lead
1315 to MIF not being zero if resolved over the thickness of the distal layer. It is known that a
1316 non-zero MIF can occur following volcanic eruptions due to time dependent movement
1317 of sulfur between changing sulfur reservoirs in the atmosphere (e.g. Pavlov et al., 2005).

1318 It is not clear if SO_3 or SO_2 was the dominant sulfur bearing gas in the ejecta plume.
1319 However, the gas phase reaction of SO_3 and water is not a simple reaction as often



1320 abbreviated in papers about atmospheric sulfur chemistry, but instead involves water
1321 vapor clusters or SO₃ adducts. Sulfur dioxide is observed to convert to particulates with
1322 an e-folding time of less than one month for moderate-sized volcanic eruptions such as
1323 the Mt. Pinatubo eruption. Following the K-Pg impact sulfur dioxide or trioxide gas may
1324 have had an extended lifetime in the atmosphere, due to the lack of sunlight to drive
1325 chemical reactions to convert it to sulfates. Clastics and nano-particles and soot, may
1326 have coagulated to large sizes and fallen out over a year or two. Alternatively, the sulfur
1327 gases may have reacted quickly on all the surfaces present, particularly in hot water
1328 present in the hot radiating layer when the ejecta reentered. Pope (1997) and Pierazzo et
1329 al. (2003) have pointed out the possible importance of the extended lifetime of the sulfate
1330 to causing a prolonged period without photosynthesis in the oceans. However, clastics or
1331 soot needed to be present in the sulfate to achieve the loss of sunlight. Recent work on the
1332 Toba eruption (Timmerick et al., 2010) shows that large sulfur injections do not produce
1333 proportionately larger climate perturbations because the climate effects of sulfur
1334 injections are self-limiting, as originally shown by Pinto et al. (1994) and recognized by
1335 Pope (1997) and Pierazzo et al. (2003). Toba probably injected an amount of sulfur
1336 dioxide within an order of magnitude of that from the K-Pg impact. Larger particles have
1337 smaller optical depths, and shorter lifetimes, than smaller particles that result from
1338 smaller SO₂ injections. Further work is needed to understand the chemistry of the sulfur
1339 injected by the Chicxulub impact to determine if it was a significant factor in the
1340 extinction event.

1341 Table 2 shows that significant injections of various ozone destroying chemicals such as
1342 NO_x, Cl, Br, and I, likely occurred. The effects of these gases need to be considered in
1343 calculations but, given the expected darkness, photochemistry may have ceased until the
1344 atmosphere cleared.

1345 Table 3 suggests that the much smaller mass injections from the impact of a 1 km
1346 diameter asteroid on land may produce optical depths that may still be important.
1347 Climate models are needed to fully evaluate these perturbations. At first glance the
1348 injections seem small. For example, the sulfur injection is only about 4 times larger than
1349 that from the Pinatubo eruption. However, the soot injection is very large. Robock et al.
1350 (2007a) and Mills et al. (2014) examined smoke injections at the tropopause of about one
1351 third the 1 km asteroid injection near the tropopause and found that the ozone layer was
1352 severely damaged, and low enough temperatures resulted to damage crops for a decade
1353 after the injection. Table 4 also indicates significant injections of iodine, which may
1354 further damage the ozone layer.

1355 About 50 1-km impacts might have occurred since the demise of the dinosaurs. Based on
1356 the fraction of Earth covered by water, about 35 of these would be expected to have hit
1357 the oceans, perhaps resulting in large ozone losses as discussed by Pierazzo et al. (2010).
1358 Each of the 15 impacts that occurred on land might have led to significant injections of
1359 nano-particles. Paquay et al. (2008) recognized the osmium signature of two large
1360 impacts in the Late Eocene, which produce the 100 km diameter craters at Popigai and
1361 Chesapeake Bay. The osmium indicates a substantial input of vaporized impactor to the
1362 atmosphere from collisions of asteroids larger than 1 km in diameter. Climate model
1363 simulations are needed to evaluate the climate changes that might have occurred. The
1364 effects could have been variable for a variety of reasons, including variability in the light



1365 absorbing properties of rock from differing objects. To have injected significant amounts
1366 of smoke the impactor would need to hit a tropical forest, or at least a heavily forested
1367 region. About 26% of the world is currently forested; about 6% is in tropical rain forest.
1368 Forested area has greatly declined. Tropical rainforests might have covered as much as
1369 20% of the Earth until recently. Hence, about 3 1-km objects might have hit a tropical
1370 rainforest and injected significant amounts of smoke since the K-Pg event.

1371 In this work we have established a set of initial conditions (Tables 1-4) that may be used
1372 for modeling the climate and air chemistry after the K-Pg impact, or the impact of a 1 km
1373 asteroid. Other authors have considered some of these initial conditions, but some, such
1374 as the nano-particles from the vaporized impactor, have not been previously studied in
1375 the detail needed to fully evaluate their importance. Much more work is needed to obtain
1376 field data to further constrain some of parameters, and to resolve remaining differences of
1377 opinion about some of the values. However, simulations using these initial conditions can
1378 now be conducted with modern models of climate and atmospheric chemistry, which
1379 should shed light on the environmental conditions at the K-Pg boundary and the dangers
1380 posed by future impacts. We recently completed such simulations using the Whole
1381 Atmosphere Community Climate Model (WACCM) at the National Center for
1382 Atmospheric Research.

1383 **Author contributions:** Owen Toon worked to compile the particle and gas emissions.
1384 Charles Bardeen tested them in a climate model to determine if the initial conditions were
1385 specified completely. Rolando Garcia considered the gases that would be important for
1386 atmospheric chemistry.

1387 **Acknowledgements:** We thank Wendy Wolbach for helpful comments about soot. C.
1388 Bardeen and R. Garcia were funded by NASA Exobiology grant #08-EXOB08-0016. The
1389 University of Colorado supported O. B. Toon's work.
1390

1391 **References**

1392

1393 Ahrens, T. J., and O’Keefe, J. D.: Impact of an asteroid or comet in the ocean and
1394 extinction of terrestrial life, Proc. Lunar Planet. Sci. Conf., 13th, Part 2, J. Geophys.
1395 Res., 88, suppl., A799–A806, 1983.

1396 Alvarez, L., Alvarez, W., Asaro, F. and Michel, H. V.: Extraterrestrial cause for the
1397 Cretaceous-Tertiary extinction, Science, 208, 1095–1108, 1980.

1398 Andreae, M. O. and Merlet, P.: Emission of trace gases and aerosols from biomass
1399 burning, Global Biogeochem. Cycles, 15, 955-966, 2001.

1400 Artemieva, N. and J. Morgan, J.: Modeling the formation of the K-Pg boundary layer,
1401 Icarus, 201, 768-780, 2009.

1402 Bardeen, C. G., Toon, O.B., Jensen, E.J., Marsh, D.R. and Harvey, V.L.: Numerical
1403 simulations of the three-dimensional distribution of meteoric dust in the mesosphere
1404 and upper stratosphere, J. Geophys. Res., 113, D17202, doi:10.1029/2007JD009515,
1405 2008.

1406 Belcher, C.M.: Reigniting the Cretaceous-Paleogene firestorm debate: Geology, 37,
1407 1147-1148, doi: 10.1130/focus122009.1, 2009.

1408 Belcher, C.M., Collinson, M.E., Sweet, A.R., Hildebrand, A.R. and Scott, A.C.: Fireball
1409 passes and nothing burns—The role of thermal radiation in the Cretaceous–Tertiary
1410 event: Evidence from the charcoal record of North America: Geology, 31, 1061–
1411 1064, doi: 10.1130/G19989.1, 2003.

1412 Belcher, C.M., Collinson, M.E., Sweet, A.R., Hildebrand, A.R. and Scott, A.C.: Reply to
1413 Comment “Fireball passes and nothing burns. The role of thermal radiation in the K/T
1414 event: Evidence from the charcoal record of North America”, Geology, Online forum,
1415 2004.

1416 Belcher, C.M., Collinson, M.E. and Scott, A.C.: Constraints on the thermal energy
1417 released from the Chicxulub impactor: New evidence from multimethod charcoal
1418 analysis: Geological Society [London] Journal, 162, 591–602, doi: 10.1144/0016-
1419 764904-104, 2005.

1420 Belcher, C.M., Finch, P., Collinson, M.E., Scott, A.C. and Grassineau, N.V.:
1421 Geochemical evidence for combustion of hydrocarbons during the K-T impact event:
1422 National Academy of Sciences Proceedings, 106, 4112–4117, doi:
1423 10.1073/pnas.0813117106, 2009.

1424 Berndt, J., Deutsch, A., Schulte, P. and Mezger, K.: The Chicxulub ejecta deposit at
1425 Demerara Rise (western Atlantic): Dissecting the geochemical anomaly using laser
1426 ablation-mass spectrometry, Geology, 39, 279-282, 2011.

1427 Bhandari, N., Verma, H. C., Upadhyy, C., Tripathi, A. and Tripathi, R. P.: Global
1428 occurrence of magnetic and superparamagnetic iron phases in Cretaceous-Tertiary
1429 boundary clays, Geolog. Soc. Am. Special Paper 356, Catastrophic Events and Mass
1430 Extinctions: Impacts and Beyond, C. Koeberl and K. G. MacLleod eds., 2002.

1431 Birks, J. W., Crutzen, P. J., and Roble, R. G.: Frequent ozone depletion resulting from



- 1432 impacts of asteroids and comets. In Bobrowsky, P., Rickman, H. (Eds).
1433 Comet/Asteroid Impacts and Human Society, Springer Pub., Berlin, 225-245, 2007.
- 1434 Bond, T. C. and Bergstrom, R. W.: Light absorption by carbonaceous particles: An
1435 investigative review, *Aerosols Sci. Tech.*, 40, 27-67, 2006.
- 1436 Bohor, B.F.: Shock-induced microdeformations in quartz and other mineralogical
1437 indications of an impact event at the Cretaceous-Tertiary boundary: *Tectonophysics*,
1438 171, 359–372, doi: 10.1016/0040-1951(90)90110-T,1990.
- 1439 Bohor, B. F, Triplehorn, D. M., Nichols, D. J. and Millard, Jr., H. T.: Dinosaurs,
1440 spherules, and the “magic layer”: A new K-T boundary clay site in Wyoming,
1441 *Geology*, 15, 896-899, 1987.
- 1442 Bohor, B. F. and Glass, B. P.: Origin and diagenesis of K/T impact spherules-From Haiti
1443 to Wyoming and beyond, *Meteoritics* 30, 182-198, 1995.
- 1444 Bosch, H., Camy-Peyret, C., Chipperfield, M. P., Fitzenberger, R., Harder, H., Platt, U.
1445 and Pfeilsticker, K.: Upper limits of stratospheric IO and OIO inferred from center-to-
1446 limb-darkening-corrected balloon-borne solar occultation visible spectra:
1447 Implications for total gaseous iodine and stratospheric ozone, *J. Geophys. Res.*, 108,
1448 D15,4455, doi:10.1029/2002JD003078, 2003.
- 1449 Boslough, M.B. and Crawford, D. A.: *Annals New York Acad. Sci.*, 822, 236-282,
1450 doi: 10.1111/j.1749-6632.1997.tb48345, 1997.
- 1451 Ciaus, P., et al.: Carbon and Other Biogeochemical Cycles, in *Climate Change 2013: The*
1452 *Physical Science Basis. Contribution of Working Group I to the Fifth Assessment*
1453 *Report of the Intergovernmental Panel on Climate Change (Stocker et al. eds.)*
1454 *Cambridge University Press, Cambridge, United Kingdom and New York, N.Y.,*
1455 *USA, 2013.*
- 1456 Crutzen, P. J., Galbally, I. E. and Bruhl, C.: Atmospheric effects from post-nuclear fires,
1457 *Climate Change*, 6, 323-364, 1984.
- 1458 Dorf, M., Butler, J. H., Butz, A., Camy-Peyret, C., Chipperfield, M. P., Kritten, L.,
1459 Montzka, S. A., Simmes, B., Weidner, F. and Pfeilsticker, K.: Long-term
1460 observations of stratospheric bromine, *Geophys. Res. Lett.*, 33, L24803,
1461 doi:10.1029/2006GL027714, 2006.
- 1462 Durant, A. J., Rose, W. I., Sarna-Wojcicki, A. M., Carey, S. and Volentik, A. C. M.:
1463 Hydrometeor-enhanced tephra sedimentation: Constraints from the 18 May 1980
1464 eruption of Mount St. Helens, *J. Geophys. Res.* 114, B03204,
1465 doi:10.1029/2008JB005756, 2009.
- 1466 Ferrow, E., Vajda, V., Koch, C. B., Peucker-Ehrenbrink, B., and Willumsen, P. S.:
1467 Multiproxy analysis of a new terrestrial and a marine Cretaceous-Paleogene (K-Pg)
1468 boundary site from New Zealand, *Geochim. et Cosmochim. Acta*, 75, 657-672, 2011.
- 1469 Folch, A., Costa, A., Durant, A. and Macedonio, G.: A model for wet aggregation of ash
1470 particles in volcanic plumes and clouds: 2. Model application, *J. Geophys. Res.*, 115,
1471 B09202, doi10.1029/2009JB007176, 2010.
- 1472 Glass B. P. and Simonson B. M.: Distal impact ejecta layers: spherules and more.



- 1473 Elements 8, 43–48, 2012.
- 1474 Goldin, T.J. and Melosh, H.J.: Self-shielding of thermal radiation by Chicxulub impact
1475 ejecta: Firestorm or fizzle?: *Geology*, 37, 1135–1138, doi: 10.1130/G30433A.1, 2009.
- 1476 Goles, G. G., Greenland L. P. and Jerome, D. Y.: Abundances of chlorine, bromine and
1477 iodine in meteorites, *Geochim. Cosmochim. Acta*, 31,1771–1787, 1967.
- 1478 Guo, S., Bluth, G. J. S., Rose, W. I., Watson, I. M. and Prata, A. J.: Re-evaluation of SO₂
1479 release of the 15 June 1991 Pinatubo eruption using ultraviolet and infrared satellite
1480 sensors, *Geochem. Geophys. Geosyst.*, 5, Q04001, doi:10.1029/ 2003GC000654,
1481 2004.
- 1482 Gulik, S. P., et al. Importance of pre-impact crustal structure for the asymmetry for the
1483 Chicxulub impact structure, *Nature Geosci.*, 1, 131–135, 2008.
- 1484 Harvey, M.C., Brassell, S.C., Belcher, C.M., and Montanari, A.: Combustion of fossil
1485 organic matter at the Cretaceous–Paleogene (K–P) boundary, *Geology*, 36, 355–358,
1486 doi:10.1130/G24646A.1, 2008.
- 1487 Hervig, M. E., Gordley, L. L., Deaver, L. E., Siskind, D. E., Stevens, M. H., Russell III,
1488 J. M., Bailey, S. M., Megner, L. and C. G. Bardeen.: First Satellite Observations of
1489 Meteoric Smoke in the Middle Atmosphere, *Geophys. Res. Lett.*, 36, L18805,
1490 doi:10.1029/2009GL039737, 2009.
- 1491 Hildebrand, A. R.: The Cretaceous/Tertiary boundary impact (or the dinosaurs didn't
1492 have a chance), *J. Roy. Astron. Soc. Can.*, 87, 77–118, 1993.
- 1493 Houghton, R. A.: Above ground forest biomass and the global carbon balance, *Global
1494 Change Biology*, 11, 945–958, 2005.
- 1495 Hunten, D. M., Turco, R. P., and Toon, O. B.: Smoke and dust particles of meteoric
1496 origin in the mesosphere and stratosphere, *J. Atmos. Sci.*, 37, 1342–1357, 1980.
- 1497 Ivany, L.C. and Salawitch, R. J.: Carbon isotopic evidence for biomass burning at the K-
1498 T boundary, *Geology*, 21, 487–490, 1993.
- 1499 Johnson B. C. and Melosh H. J.: Impact spherules as a record of an ancient heavy
1500 bombardment of Earth, *Nature* 485, 75–77, 2012a.
- 1501 Johnson, B. C., and Melosh, H. J.: Formation of spherules in impact produced vapor
1502 plumes, *Icarus*, 217, 416–430, 2012b.
- 1503 Johnson, B. C., and Melosh, H. J.: Formation of melt droplets, melt fragments, and
1504 accretionary impact lapilli during hypervelocity impact, *Icarus*, 228, 347–363, 2014.
- 1505 Jones, E. M. and Kodis, J. W.: Atmospheric effects of large body impacts: The first few
1506 minutes, in *Geological Implications of Impacts of Large Asteroids and Comets on the
1507 Earth*, edited by L. T. Silver and P. H. Schultz, *Geol. Soc. Am. Special Paper* 190,
1508 175–186, 1982.
- 1509 Kalashnikova, O., Horanyi, M., Thomas, G. E. and Toon, O. B.: Meteoric smoke
1510 production in the atmosphere, *Geophys. Res. Lett.*, 27, 3293–3296, 2000.
- 1511 Kallemeyn, G. W. and Wasson, J. T.: The compositional classification of chondrites-I.



- 1512 The carbonaceous chondrite groups, *Geochim. Cosmochim. Acta* 45, 1217-1230,
1513 1981.
- 1514 Kring, D. A., and Durda, D. D.: Trajectories and distribution of material ejected from the
1515 Chicxulub impact crater: Implications for post impact wildfires, *J. Geophys. Res.*,
1516 107, E8, 5062, doi:10.1029/2001JE001532, 2002.
- 1517 Kring, D. A., Melosh, H. J. and Hunten, D. M.: Impact-induced perturbations of
1518 atmospheric sulfur, *Earth Planet. Sci. Lett.*, 14, 201-212, 1996.
- 1519 Lack, D. A., Bahreini, R., Cappa, C. D., Middlebrook, A. M. and Schwartz, J. P.: Brown
1520 carbon and internal mixing in biomass burning particles, *Pub. Nat. Acad. Sci.*, 109,
1521 14802-14807, 2012.
- 1522 Malone, R. C., Auer, L., Glatzmaier, G., Wood, M. and Toon, O. B.: Influence of Solar
1523 Heating and Precipitation Scavenging on the Simulated Lifetime of Post-Nuclear War
1524 Smoke, *Science*, 230, 317-319, 1985.
- 1525 Matichuk, R. I., Colarco, P.R., Smith, J.A. and Toon, O.B.: Modeling the transport and
1526 optical properties of smoke plumes from South American biomass burning, *J.*
1527 *Geophys. Res.*, 113, D07208, doi:10.1029/2007JD009005, 2008.
- 1528 Matthews, N. E., Smith, V. C., Costa, A., Durant, A J., Pyle, D. M. and Pearce, N. J. G.:
1529 Ultra-distal tephra deposits from super-eruptions: Examples from Toba, Indonesia
1530 and Taupo Volcanic Zone, New Zealand, *Quaternary Int.* 258, 54-79, 2012.
- 1531 Melosh, H.J. and Vickery, A.M.: Melt droplet formation in energetic impact events,
1532 *Nature* 350, 494–497, 1991.
- 1533 Melosh, H.J., Schneider, N.M., Zahnle, K.J. and Latham, D.: Ignition of global wildfires
1534 at the Cretaceous–Tertiary boundary, *Nature*, 343, 251–254, 1990.
- 1535 Mikhailov, E. F., Vlasenko, S. S., Podgorny, I. A., Ramanathan, V., Corrigan, C. E.:
1536 Optical properties of soot-water drop agglomerates: An experimental study, *J.*
1537 *Geophys. Res.*, 111, D07209, doi:10.1029/2005JD006389, 2006.
- 1538 Millero, F. J., Feistel, R., Wright, D. G. and McDougall, T. J.: The composition of
1539 standard seawater and the definition of the reference composition salinity scale,
1540 *Deep-Sea Res.*, 55, 50-72, 2008.
- 1541 Mills, M. J., Toon, O. B., Turco, R.P., Kinnison, D.E. and Garcia, R.R.: Massive global
1542 ozone loss predicted following regional nuclear conflict, *P. Nat. Acad. Sci.*, 105,
1543 5307-5312, 2008.
- 1544 Mills, M. J., Toon, O. B. and Robock, A.: Multidecadal global cooling and unprecedented
1545 ozone loss following a regional nuclear conflict, *Earth's Future*, 2, 161-176,
1546 doi:10.1002/2013EF00020, 2014.
- 1547 Milne, P. H. and McKay, C.: Response of marine plankton communities to a global
1548 atmospheric darkening, in *Geological Implications of Impacts of Large Asteroids and*
1549 *Comets on the Earth*, edited by L. T. Silver and P. H. Schultz, *Geol. Soc. Am. Special*
1550 *Paper* 190, 297-303, 1982.
- 1551 Morgan, J., Artemieva, N., and Goldin, T.: Revisiting wildfires at the K-Pg boundary, *J.*



- 1552 Geophys. Res. Biogeosci., 118, 1-13, doi:10.1002/2013JG002428, 2013.
- 1553 Nassar, R., et al.: A global inventory of stratospheric chlorine in 2004, *J. Geophys. Res.*,
1554 111, D22312, doi:10.1029/2006JD007073, 2006.
- 1555 Neely, R., English, J. M., Toon, O. B., Solomon, S., Mills, M. and Thayer, J. P.:
1556 Implications of extinction due to meteoritic smoke in the upper stratosphere,
1557 *Geophys. Res. Lett.*, 38 L24808, doi 10.1029/2011GL049865, 2011.
- 1558 O’Keefe, J.D. and Ahrens, T.J.: The interaction of the Cretaceous/Tertiary Extinction
1559 Bolide with the atmosphere, ocean, and solid Earth, in *Geological Implications of*
1560 *Impacts of Large Asteroids and Comets on the Earth*, edited by L. T. Silver and P. H.
1561 Schultz, *Geol. Soc. Am. Spec. Pap.* 190, 103–120, 1982.
- 1562 Orofino, V., Blanco, A., Fonti, S., Proce, R. and Rotundi, A.: The infrared optical
1563 constants of limestone particles and implications for the search of carbonates on
1564 Mars, *Planet. Space Sci.*, 46, 1659-1669, 1998.
- 1565 Pan, Y., et al.: A large and persistent carbon sink in the world’s forests, *Science*, 333,
1566 988-993, 2011.
- 1567 Paquay F. S., Ravizza G. E., Dalai T. K. and Peucker-Ehrenbrink B.: Determining
1568 chondritic impactor size from the marine osmium isotope record. *Science* 320, 214–
1569 218, 2008.
- 1570 Parkos, D., Alexeenko, A., Kulakhmetov, M., Johnson, B. C., and Melosh, H. J.: NO_x
1571 production and rainout from Chicxulub impact ejecta and reentry, *J. Geophys. Res. –*
1572 *Planets*, 120, doi 10.1002/2015JE004857, 2015.
- 1573 Pavlov, A.A., Mills, M.J. and Toon, O. B.: Mystery of the volcanic mass-independent
1574 sulfur isotope fractionation signature in the Antarctic ice-core, *Geophys. Res. Lett.*,
1575 32, L12816, doi:10.1029/2005GL022784, 2005.
- 1576 Penner, J. E., Haselman, Jr., L.C. and Edwards, L. L.: Smoke-plume distributions above
1577 large-scale fires: Implications for simulations of “Nuclear Winter”, *J. Climate and*
1578 *Appl. Meteor.*, 25, 1434-1444, 1986.
- 1579 Pierazzo, E., Hahmann, A. N. and Sloan, L.C.: Chicxulub and climate: Radiative
1580 perturbations of impact-produced S-bearing gases, *Astrobio.*, 3, 99-118, 2003.
- 1581 Pierazzo, E., Garcia, R. R., Kinnison, D. E., Marsh, D. R., Lee-Taylor, J. and Crutzen, P.
1582 J.: Ozone perturbation from medium-sized asteroid impacts in the ocean, *Earth and*
1583 *Planet Sci. Lett.*, doi:10.1016/j.epsl.2010.08.036, 2010.
- 1584 Pierazzo, E. and Artemieva, N.: Local and global environmental effects of impacts on
1585 Earth, *Elements*, 8, 55-60, 2012.
- 1586 Pittock, A. B., Ackerman, T. P., Crutzen, P. J., MacCracken, M. C., Shapiro, C. S., and
1587 Turco, R. P.: *Environmental Consequences of Nuclear War SCOPE-28, Vol. 1,*
1588 *Physical and Atmospheric Effects*, Wiley, Chichester, England, 1985 (Second ed.
1589 1989).
- 1590 Pinto J.R., Turco R.P., Toon, O.B.: Self-limiting physical and chemical effects in
1591 volcanic eruption clouds, *J. Geophys. Res.*, 94, 11165–11174, doi:10.1029/



- 1592 JD094iD08p11165, 1989.
- 1593 Pollack, J.B., Toon, O. B., Ackerman, T. P., McKay, C. P. and Turco, R. P.:
1594 Environmental effects of an impact generated dust cloud: Implications for the
1595 Cretaceous-Tertiary extinctions, *Science*, 219, 287-289, 1983.
- 1596 Pope, K. O.: Impact dust not the cause of the Cretaceous-Tertiary mass extinction,
1597 *Geology*, 30, 99-102, 2002.
- 1598 Pope, K. O., Baines, K. H., Ocampo, A. C. and Ivanov, B. A.: Energy, volatile
1599 production, and climatic effects of the Chicxulub Cretaceous/Tertiary impact, *J.*
1600 *Geophys. Res.*, 102, 21645-21664, 1997.
- 1601 Premovic, P. I.: Soot in Cretaceous-Paleogene boundary clays worldwide: Is it really
1602 derived from fossil fuel beds close to Chicxulub?, *Centra. European J. Geosci.*, 4,
1603 383-387, 2012.
- 1604 Pueschel, R. F., Russell, P. B., Allen, D. A., Ferry, G. V., Snetsinger, K. G., Livingston,
1605 K. G. and Verma, S.: Physical and optical properties of the Pinatubo volcanic aerosol:
1606 Aircraft observations with impactors and a Sun-tracking photometer, *J. Geophys.*
1607 *Res.*, 99, 12,915-12,922, 1994.
- 1608 Querry, M. R., Osborne, G., Lies, K., Jordon, R. and Covey, R. M.: Complex refractive
1609 index of limestone in the visible and infrared, *Applied Optics*, 17, 353-356, 1978.
- 1610 Renne, P. R., et al.: Time scales of critical events around the Cretaceous-Paleogene
1611 boundary, *Science*, 339, 684-687, 2013.
- 1612 Robertson, D.S., McKenna, M.C., Toon, O.B., Hope, S. and Lillegraven, J.A.: Survival in
1613 the first hours of the Cenozoic: *Geological Society of America Bulletin*, 116, 760–
1614 768, doi: 10.1120/B25402.1, 2004.
- 1615 Robertson, D. S., Lewis, W. M., Sheehan, P. M. and Toon, O. B.: K-Pg extinction:
1616 Reevaluation of the heat-fire hypothesis, *J. Geophys. Res.*, 118, 329-336,
1617 doi10.1002/jgrg.20018, 2013a.
- 1618 Robertson, D. S., Lewis, W. M., Sheehan, P. M. and Toon, O. B.: K-Pg extinction
1619 patterns in marine and freshwater environments: The impact winter model, *J.*
1620 *Geophys. Res.*, 118, 1006-1014, doi10.1002/jgrg.20086, 2013b.
- 1621 Robock, A., Oman, L., Stenchikov, G.L., Toon, O. B., Bardeen, C. and Turco, R.P.:
1622 Climatic consequences of regional nuclear conflicts, *Atmos. Chem. Phys.* 7, 1973-
1623 2002, 2007a.
- 1624 Robock, A., Oman, L., and Stenchikov, G. L.: Nuclear winter revisited with a modern
1625 climate model and current nuclear arsenals: Still catastrophic consequences, *J.*
1626 *Geophys. Res.*, 112, D13107, doi:10.1029/2006JD008235, 2007b.
- 1627 Rose, W. I. and Durant, A. J.: Fine ash content of explosive eruptions, *J. Volcan.*
1628 *Geothermal Res.*, 186, 32-39, 2009.
- 1629 Schmidt, A., et al.: Selective environmental stress from sulfur emitted by continental
1630 flood basalt eruptions, *Nature Geosci.*, 9, 77-82, 2016.
- 1631 Schulte, P., Deutsch, A., Salge, T., Berndt, J., Kontny, A., MacLeod, K. G., Neuser, R. D.



- 1632 and Krumm, S.: *Geochim. Cosmochim. Acta*, 73,1180-1204, 2008.
- 1633 Schulte, P. et al.: The Chicxulub Asteroid Impact and Mass Extinction at the Cretaceous-
1634 Paleogene Boundary, *Science*, 327, 1214-1218, doi: 10.1126/science.1177265, 2010.
- 1635 Small, R. D. and Heikes, K. E.: Early cloud formation and large area fires, *J. Appl.*
1636 *Meteorol.*, 27, 654–663, 1988.
- 1637 Smit, J.: The global stratigraphy of the Cretaceous-Tertiary boundary impact ejecta, *Ann.*
1638 *Rev. Earth Planet. Sci.*, 27, 75-113, 1999.
- 1639 Stothers, R. B.: The great Tambora eruption in 1815 and its aftermath, *Science*, 224,
1640 1191-1198, 1984.
- 1641 Timmreck C., Graf, H. F., Lorenz, S. J., Niemeier, U., Zanchettin, D., Matei, D.,
1642 Jungclaus, J. H., Crowley, T.J.: Aerosol size confines climate response to volcanic
1643 super-eruptions, *Geophys. Res. Lett.*, 37, L24705, doi:10.1029/2010GL045464, 2010.
- 1644 Toon, O. B., and Ackerman, T. P.: Algorithms for the Calculation of Scattering by
1645 Stratified Spheres, *Appl. Optics*, 20, 3657-3660, 1981.
- 1646 Toon, O. B., Pollack, J. B., Ackerman, T.P., Turco, R.P., McKay, C.P. and Liu, M.S.:
1647 Evolution of an Impact-Generated Dust Cloud and its Effects on the Atmosphere, in
1648 *Geological Implications of Impacts of Large Asteroids and Comets on the Earth*,
1649 edited by L. T. Silver and P. H. Schultz, *Geological Soc. Am. Spec. Paper* 190, 187-
1650 200, 1982.
- 1651 Toon, O. B., Zahnle, K., Morrison, D., Turco, R. P. and Covey, C.: Environmental
1652 perturbations caused by the impacts of asteroids and comets: *Reviews of Geophysics*,
1653 35, 41-78, 1997.
- 1654 Toon, O. B., Turco, R. P., Robock, A., Bardeen, C., Oman, L. and Stenchikov, G. L.,
1655 Atmospheric effects and societal consequences of regional scale nuclear conflicts and
1656 acts of individual nuclear terrorism, *Atmos. Chem. Phys.*, 7, 1973-2002, 2007.
- 1657 Trinquier, A., Birck, J. -L., Alle`gre, C. J.: The nature of the KT impactor. A ⁵⁴Cr
1658 reappraisal, *Earth and Planet. Sci. Lett.*, 241, 780–788, 2006.
- 1659 Turco, R. P., Toon, O. B., Whitten, R. C., Hamill, P., and Keesee, R. G.: The 1980
1660 eruptions of Mt. St. Helens: Physical and chemical processes in stratospheric clouds,
1661 *J. Geophys. Res.*, 88, 5299-5319, 1983.
- 1662 Turco, R. P., Toon, O. B., Ackerman, T. P., Pollack, J.B. and Sagan, C.: Climate and
1663 smoke: An appraisal of nuclear winter, *Science*, 247, 166-176, 1990.
- 1664 Verma, H. C., Upadhyay, C., Tripathi, A., Tripathi, R. P. T. and Bhandari, N.: Thermal
1665 decomposition pattern and particle size estimate of iron minerals associated with the
1666 Cretaceous-Tertiary boundary at Gubbio, *Meteor. Planet. Sci.*, 37, 901-909, 2002.
- 1667 Vajda, V., Ocampo, A., Ferrow, E., Koch, C. B.: Nano-particles as the primary cause of
1668 long-term sunlight suppression at high latitudes following the Chicxulub impact-
1669 evidence from ejecta deposits in Belize and Mexico, *Godwana Res.*, 27, 1079-1088,
1670 2015.
- 1671 Ward, W. C., Keller, G., Stinnesbeck, W. and Adatte, T.: Yucatan subsurface



- 1672 stratigraphy: Implications and constraints for the Chicxulub impact, *Geology*, 23,
1673 873-876, 1995.
- 1674 Wdowiak, T. J., Armendarez, L. P., Agresti, D. G., Wade, M. L., Wdowiak, S. Y.,
1675 Claeys, P. and Izett, G.: Presence of an iron-rich nanophase material in the upper
1676 layer of the Cretaceous-Tertiary boundary clay, *Meteoritics Planet. Sci.*, 36, 123-133,
1677 2001.
- 1678 Wolbach, W.S., Lewis, R.S. and Anders, E.: Cretaceous extinctions: Evidence for
1679 wildfires and search for meteoritic material, *Science*, 240, 167-170, 1985.
- 1680 Wolbach, W.S., Gilmour, I., Anders, E., Orth, C.J. and Brooks, R.R.: Global fire at the
1681 Cretaceous-Tertiary boundary, *Nature*, 334, 665-669, 1988.
- 1682 Wolbach, W.S., Anders, E. and Nazarov, M. A.: Fires at the K-T Boundary: Carbon at
1683 the Sumbar, Turkmenia site, *Geochemica et Cosmochimica Acta*, 54, 1133-1146.
1684 1990.
- 1685 Wolbach, W. S., Widicus, S. and Kyte, F. T.: A search for soot from global wildfires in
1686 Central Pacific Cretaceous-Tertiary boundary and other extinction and impact horizon
1687 sediments, *Astrobio.*, 3, 91-97, 2003.
- 1688 Wolf, E. T. and Toon, O. B.: Fractal organic hazes provide an ultraviolet shield for early
1689 Earth, *Science*, 328, 1266-1268, 2010.
- 1690 Yancy, T. and Guillemette, R. N.: Carbonate accretionary lapilli in distal deposits of the
1691 Chicxulub impact event, *Geolog. Soc. Am. Bull.*, 120, 1105-1118, 2008.
- 1692 Zahnle, K.: Atmospheric chemistry by large impacts, in *Global Catastrophes in Earth
1693 History: An Interdisciplinary Conference on Impacts, Volcanism and Mass Mortality*,
1694 ed. Sharpton, V.L. and Ward, P. D., *Geolog. Soc. Am. Special Paper* 247, 271-288,
1695 1990.
1696


 1697 Table 1: K-Pg injection scenario for impactor mass $\sim 1.4 \times 10^{18}$ g, impact energy $\sim 2.8 \times 10^{23}$
 1698 $J = 6.8 \times 10^7$ Mt for 20 km/s impact

Property/ Constituent	Type 2 spherules	Soot	Nano- particles from vaporized rock	Clastics, μm distributed globally	S
Material amount, g, (g cm^{-2})	2.3×10^{18} (0.44)	7×10^{16} (1.3×10^{-2})	$\sim 2 \times 10^{18}$ (0.4)	$< 6 \times 10^{16}$ (0.01)	9×10^{16} (5.4×10^{-2} g SO_4/cm^2)
Estimated global optical depth as $1 \mu\text{m}$ particles*	~ 20 (for $250 \mu\text{m}$ particles)	~ 100	~ 2000	~ 90	~ 450
Vertical distribution	70 km as center of Gaussian distribution with half width of 6.6 km	Eq. 2	Same as Type 2 spherules	Uniformly mixed vertically above tropopause	Same as Type 2 spherules
Optical properties	Not relevant	$n=1.8$ $k=0.67$	Hervig et al., (2006)	Orofino et al. for limestone	Sulfuric acid
Initial Particle size	$250 \mu\text{m}$ diameter	Lognormal, modal particle radius $0.11 \mu\text{m}$, sigma 1.6; monomers 30-60 nm	20 nm diameter	Lognormal, modal particle radius $0.5 \mu\text{m}$, sigma 1.65	gas
Material density, g cm^{-3}	2.7	1.8	2.7	2.7	1.8

1699 *Qualitative estimate for comparison purposes only

1700



1701

1702 Table 2: Gas phase emissions (g) from the Chixculub impact

Sources/ Gases	S (10^{13})	C (as CO_2^{**}) (10^{17})	H_2O (10^{15})	Cl (10^{12})	Br (10^{10})	I (10^7)	N (10^{14})	Vertical distribution
Ambient values, g	1*	8.4	1.3 strat	2.3 strat	3.1 strat	<2.3 strat	2 as N_2O	
Impactor	4×10^3	0.3	200	7×10^2	5×10^2	7×10^4		As Type 2 spherules
Forest fires	40	6	1500	200	1000	9×10^5	10	As soot
Vaporized sea water	60	small	600	1×10^4	5×10^3	40	-	As Type 2 spherules
Splashed sea water***	500	small	5×10^3	1×10^5	4×10^4	3×10^2	-	Uniformly mixed above tropopause
Impact site (vaporized)	5000	0.6	90	800	400	3		As Type 2 spherules
Impact site (degassed)	500	0.1	120	2×10^3	1×10^3	7		Uniformly mixed above tropopause
Atmospheric heating							300 as NO_x created from air	Half uniformly mixed, half as Type 2 spherules

1703

- * Based on Pinatubo eruption

1704

- ** Mass as given in terms of C, but emission is in the form of CO_2 .

1705

- ***S, Cl, Br, I likely injected as particulates

1706



1707

1708 Table 3: 1 km land* injection scenario for impactor mass 1.4×10^{15} g; impactor energy
 1709 $\sim 2.8 \times 10^{20}$ J = 6.8×10^4 Mt

Property/ Constituent	Type 2 spherules	Soot**	Nano- particles from vaporized rock***	Clastics, $< \mu\text{m}$ distributed globally	S
Material amount g (g cm^{-2})	1.4×10^{15} (2.6×10^{-4})	2.8×10^{13} (5.6×10^{-6})	1×10^{15} (2×10^{-4})	2.6×10^{13} (5×10^{-6})	4.4×10^{13} (2.6×10^{-5} g $\text{SO}_4 \text{ cm}^{-2}$)
Estimated global optical depth as 1 μm particles	0.2 (as 15 μm particles)	4.7×10^{-2}	1.5	4×10^{-2}	0.22
Vertical distribution	Table 1 Over 50% of Earth	Table 1 Over 4×10^4 km^2	Table 1 Over 50% of Earth	Uniformly mixed above tropopause, spread over $4 \times 10^5 \text{ km}^2$	Follow nano- particles
Optical properties	Not relevant	Table 1	Table 1	Depends on impact site	Table 1
Initial particle size (μm)	$15 \mu\text{m}$	Table 1	20 nm	Table 1	

1710 *We assume a 1 km asteroid impact would not penetrate through the 5km average depth
 1711 of the ocean. Therefore, none of the materials in this Table would be injected into the
 1712 atmosphere for an ocean impact. For the density of all materials follow Table 1.

1713 **The material amount assumes an impact into a region where 2.25 g C cm^{-2} flammable
 1714 biomass is consumed. The material amount can be scaled linearly for other choices of
 1715 available biomass that burns.

1716 ***We assume about 35% of the impactor and an equivalent mass of target would vaporize
 1717 and end up as nano-particles.

1718

1719



1720 Table 4: Gas phase emissions (g) from a 1-km diameter impact

Sources/ Gases	S (10 ¹³)	C* (10 ¹⁷)	H ₂ O (10 ¹⁵)	Cl (10 ¹²)	Br (10 ¹⁰)	I (10 ⁷)	N (10 ¹⁴)	Vertical distribution
Ambient values, g	1**	8.4	1.3 strat	2.3 strat	3.1 strat	<2.3 strat	2 as N ₂ O**	
Impactor/ land only	4.4	3x10 ⁻²	0.2	0.7	0.5	68	-	As type 2 spherules
Forest fires/land only	2.7 x10 ⁻²	4x10 ⁻³	0.9	0.12	0.62	560	6.9x10 ⁻³	As soot
Vaporized sea water	0.9	small	10	200	80	0.6		Uniformly mixed
Splashed sea water***	3	small	30	600	200	2		
Atmospheric heating							0.6	Uniformly mixed

1721 * in the form of carbon dioxide

1722 ** based on Pinatubo volcanic eruption

1723 *** S, Cl, Br, I may be released as particulates.

1724



1725 Table 5: Comparison of Toon et al. (1997) and Pope (2002) estimates of submicron
 1726 clastics.

Method	Quartz based estimate-Pope (2002)	Injected mass-Toon et al. (1997)*	Injected mass - revised	Quartz based estimate-revised	1 km impactor**
Initial clastic debris, g	$<10^{16}$	7×10^{20}	2.9×10^{19}	5×10^{18}	1.3×10^{16}
% clastic $<1 \mu\text{m}$	<1	0.1	2	1	2
Submicron clastics, g	$<10^{14}$	7×10^{17}	5.8×10^{17}	5×10^{16}	2.6×10^{14}
Stratospheric submicron surviving initial removal, g	10^{14}	7×10^{17}	$<5.8 \times 10^{16}$	5×10^{16}	$< 2.6 \times 10^{13}$

1727 * assuming an impact energy of $1.5 \times 10^8 \text{ Mt}$, and a velocity of 20 km/s.

1728 ** scaled from Injected Mass Revised using energy scaling assuming an impact energy of
 1729 $6.8 \times 10^4 \text{ Mt}$

1730

1731

1732



1733 Table 6: Impactor composition, seawater composition, Yucatan impact site composition
 1734 and forest fire emission ratios

	S	C	H ₂ O	Cl	Br	I	EC	N
Carbonaceous Chondrite (g/g impactor)	3.1 x10 ⁻²	1.98 x10 ⁻²	11.9 x10 ⁻²	4.7 x10 ⁻⁶	3.27 x10 ⁻⁶	4.8 x10 ⁻⁷		
Sea water (g/g sea water)	9.1 x10 ⁻⁴	3 x10 ⁻⁶	0.965	1.9 x10 ⁻²	8.2 x10 ⁻⁵	6.0 x10 ⁻¹⁰	-	-
Impact site (g/g site)	7.1 x10 ⁻²	9.6 x10 ⁻²	0.07					
Emission ratios for forest fires g/g of dry biomass burned	2.9 x10 ^{-4*}	4.3 x10 ⁻¹ as CO ₂ 4.4 x10 ⁻² as CO 5.1 x10 ⁻³ as CH ₄	Highly variable, can equal dry weight	As CH ₃ Cl 1.4 x10 ⁻⁵ to 1.3 x10 ⁻⁴	As CH ₃ Br 6.7 x10 ⁻⁶	As CH ₃ I 6.1 x10 ⁻⁶	6.6 x10 ^{-4**}	7.5 x10 ⁻⁴ as NO 6 x10 ⁻⁵ as N ₂ O

1735 *The mass is given in terms of S, but the emission is in the form of SO₂.

1736 ** We used 0.03 g/g in Table 3, because forest fires will not produce as much soot as mass
 1737 fires.

1738



1739 Table 7 Suggestions for data collection

Property of interest	Rationale
Global distribution of spherules	Some impact models suggest spherules were not distributed globally, limiting area of Earth that might experience fire ignition
Number concentration, size of spherules	Current data are incomplete on number and size of spherules
Soot distribution	Profile soot/iridium/spherule distribution to determine if fires are contemporaneous with iridium fallout
Nano-meter material	Nano-meter material has been detected, but its mass needs to be quantified
Clastics	Submicron component not detected. Possibly search for micron/submicron shocked quartz.
Sulfur	Use sulfur isotopes to search for extraterrestrial sulfur, sulfur MIF to test for prolonged lifetime

1740

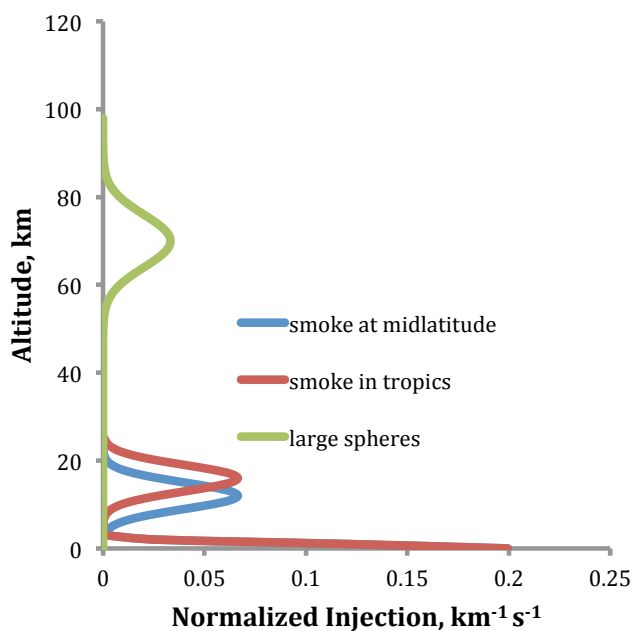


Figure 1. Injection profiles for smoke at midlatitudes and the tropics and for large spherical particles. Many other constituents follow the same vertical profiles as noted in Table 1-4. We suggested clastics be placed above the tropopause using a constant mixing ratio.

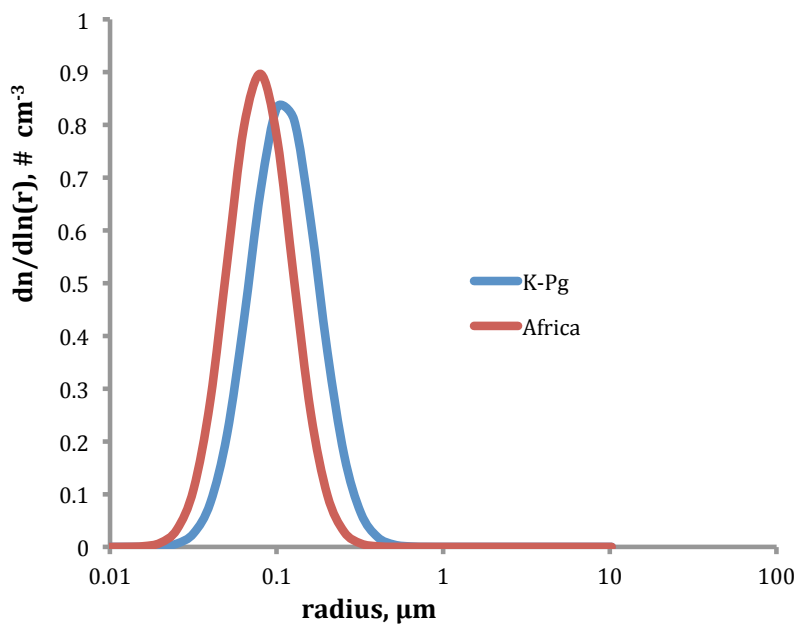


Fig. 2. The size distributions for smoke from modern fires in Africa, and from the K-Pg boundary layer (Wolbach et al., 1985; Matichuk et al., 2008)

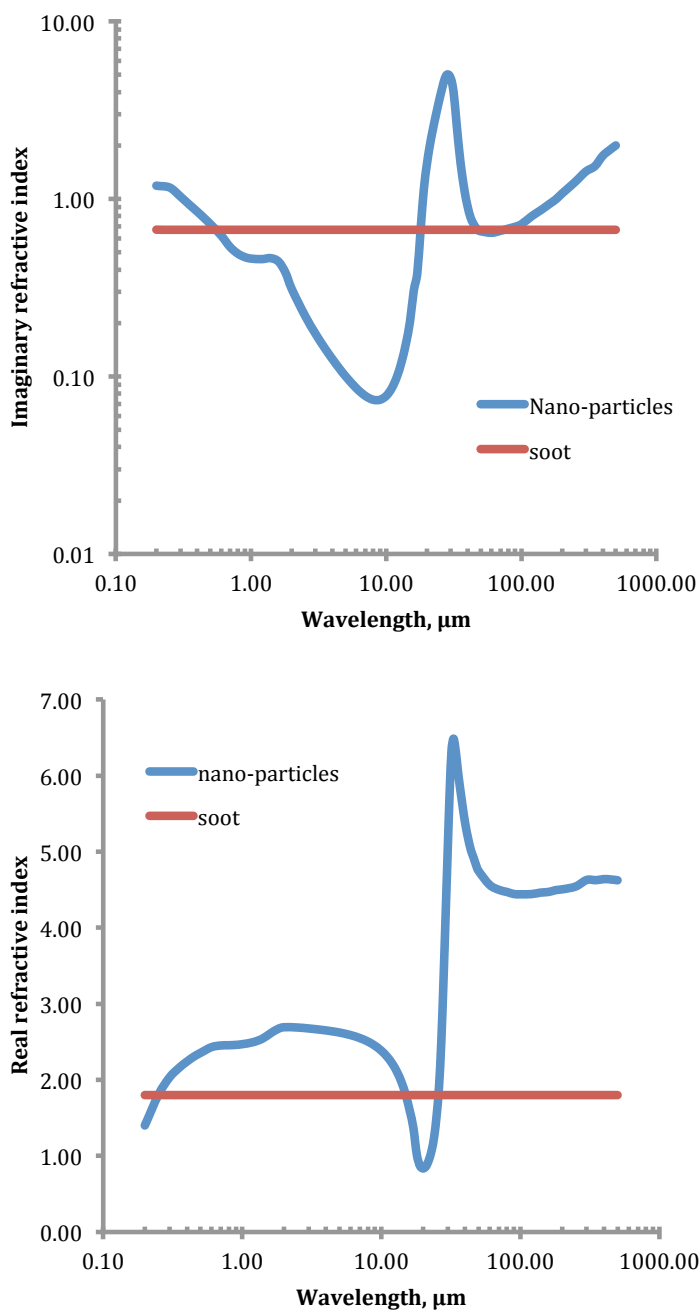


Fig. 3 The real and imaginary parts of the refractive index suggested for nano-particles, and for soot.